Transcriptomic insights into the tripartite plant–pathogen–mycoparasite interaction reveal novel mechanisms involving fungal secretomes and plant amino acid metabolism

Kazuya Maeda[1], Mariko Kouda[1], Mai Ohara[1], Takumi Kawase[1], Koki Saito[1], Eishin Iwao[1], Hirotoshi Sushida[2], Tomoko Suzuki[3], Takuya Sumita[4], Yuichiro Iida[1]

[1] Laboratory of Plant Pathology, Faculty of Agriculture, Setsunan University, Nagaotoge-cho 45-1, Hirakata, Osaka 573-0101, Japan

[2] Institute of Food Research, National Agriculture and Food Research Organization (NARO), 2-1-12 Kannondai, Tsukuba, Ibaraki 305-8642, Japan

[3] Department of Chemical and Biological Sciences, Faculty of Science, Japan Women's University, Mejirodai 2-8-1, Bunkyo-ku, Tokyo 112-8681, Japan

[4] Department of biological resources management, School of Environmental Science, The University of Shiga Prefecture, Hassaka-cho 2500, Hikone, Shiga 522-8533

[*] **Correspondence to Y. Iida (yuichiro.iida@setsunan.ac.jp)**

Present address (Mariko Kouda): Graduate School of Human Sciences, Kobe College, Okadayama 4-1, Nishinomiya, Hyogo, 662-8505, Japan

Short title: Transcriptomic analysis among plant, pathogen and mycoparasite

ORCIDs: Kazuya Maeda: 0000-0001-9858-0362; Mariko Kouda: 0009-0000-8862-4202; Takumi Kawase: 0009-0006-2448-0805; Koki Saito: 0009-0007-5348-7739; Eishin Iwao: 0009-0000-6697-5378; Hirotoshi Sushida: 0000-0003-0631-6068; Tomoko Suzuki: 0000-0001-9561-968X; Takuya Sumita: 0000-0001-7980-018X; Yuichiro Iida: 0000-0001-5062-3255.

Word Count

Introduction: 905

Materials and Methods: 2,094

Results: 2,484

Discussion: 1,964

Total: 7,447

Number of Figures, Tables, and Supporting Information

Figures: 8 (all to be published in colour)

Tables: 0

Supporting Information: 18

Summary

· The tomato–*Cladosporium fulvum* (syn. *Fulvia fulva*) pathosystem has served as a model for the gene-for-gene concept of effectors and resistance proteins, but this binary framework does not include the potential influence of other microbial participants. Here, we discovered a unique mechanism involved in the tripartite interaction among *C. fulvum*, its mycoparasitic fungus *Hansfordia pulvinata*, and host tomato plant.

· Transcriptomic analyses of under mycoparasitic conditions *in planta* and *in vitro* revealed that in *H. pulvinata* genes encoding small secreted proteins were upregulated during mycoparasitism. Notably, a Nep1-like protein (HpNlp1) lacked typical necrosis-inducing activity but induced the accumulation of antifungal substances in the plant apoplast, inhibiting spore germination of *C. fulvum.*

· In *C. fulvum* parasitized by *H. pulvinata*, effector genes were highly expressed. Strikingly, effector protein Ecp2 was found to share structural similarity with pathogen killer toxin 4 proteins and had broad-spectrum antifungal activity, indicating a dual function in fungal competition and *Cf-ECP2*-mediated plant resistance.

· In tomato plants, when *C. fulvum* was parasitized by *H. pulvinata*, amino acid biosynthetic pathways and defense-related genes were exclusively activated. These results suggest that in the tripartite molecular network, the mycoparasite simultaneously suppressed the pathogen and induced plant resistance. In this newly discovered multilayered molecular network, the mycoparasite coordinates pathogen suppression and plant defense within the tripartite interaction.

Keywords: mycoparasitism, Nep1-like protein, Ecp2 effector, antifungal proteins, amino acid metabolisms, *Cladosporium fulvum*, *Hansfordia pulvinata*, *Solanum lycopersicum*

67

68 **INTRODUCTION**

69 The biotrophic filamentous fungus *Cladosporium fulvum* Cooke [syn. *Fulvia fulva* (Cooke)
70 Cif.] causes tomato leaf mold, a serious economic threat due to reduced fruit yield and quality
71 and occasional death of the tomato plant (*Solanum lycopersicum* L.) (Thomma *et al*., 2005;
72 de Wit *et al*., 2009). The fungus enters tomato leaves through open stomata in high humidity,
73 colonizes the apoplast, and secretes numerous effector proteins to suppress plant immunity
74 and facilitate infection (Mesarich *et al*., 2023). Commercial tomato cultivars have thus been
75 bred with *Cf* resistance genes encoding receptor-like proteins (RLPs) with extracytoplasmic
76 leucine-rich repeats from wild relatives (Mesarich *et al*., 2023). These RLPs recognize the
77 corresponding *C. fulvum* effector proteins as virulence factors via a gene-for-gene
78 relationship and trigger a hypersensitive response to restrict the growth of *C. fulvum*
79 (Mesarich *et al*., 2023). However, new races of *C. fulvum* can rapidly evolve through
80 mutation or loss of effector genes and evade plant immunity (Iida *et al*., 2015; de la Rosa *et*
81 *al*., 2024). The extensive use of resistant cultivars carrying only one or a few *Cf* genes has
82 consequently led to the emergence of *C. fulvum* races that can overcome the resistance of the
83 tomato plants (Luderer *et al*., 2002; Mesarich *et al*., 2014).

84 To date, over 100 effector genes have been identified in *C. fulvum* (Mesarich *et al*., 2018;
85 Zaccaron & Stergiopoulos, 2024). Most encode small cysteine-rich proteins that contain an
86 N-terminal signal peptide for secretion. The identified avirulence (Avr) and extracellular
87 proteins (Ecp) effectors—such as Avr2, Avr4, Avr4E, Avr5, Avr6 (Ecp5), Avr9B, Avr9C,
88 Ecp1, Ecp2, Ecp4, and Ecp6—exemplify the complex coevolution between fungal virulence
89 factors and their cognate *Cf* immune receptors (Wulff *et al*., 2009; de la Rosa *et al*., 2024;
90 Shol *et al*. 2025). Several effectors have been functionally characterized. Avr2 acts as a
91 cysteine protease inhibitor that targets the apoplastic cysteine proteases Rcr3 and Pip1,
92 thereby interfering with basal defense mechanisms conserved across solanaceous plants
93 (Rooney *et al*., 2005; Shabab *et al*., 2008; Kourelis *et al*., 2020). Ecp6 suppresses chitin-
94 triggered immunity by sequestering chitin oligomers released from the fungal cell wall, thus
95 evading recognition by host pattern-recognition receptors (de Jonge *et al*., 2010). In
96 contrast, Ecp2 induces cell death in both tomato and nonhost plants, suggesting a dual role as
97 a potential virulence and avirulence factor (de Kock *et al*., 2004; de Wit *et al*.,
98 2012). Notably, the Ecp2 effector contains an Hce2 (homolog of *Cladosporium fulvum Ecp2*)
99 domain that is widely conserved across diverse fungal and bacterial taxa, implying a
100 fundamental role for this domain in microbe–plant interactions (Stergiopoulos *et al*., 2012).

101 However, the biochemical function of Ecp2 remains unclear. Of additional concern is that *C.*
102 *fulvum* has developed resistance to fungicides (Yan *et al*., 2008; Watanabe *et al*., 2017). The
103 extensive breakdown of the resistance conferred by single *Cf* resistance genes and the
104 emergence of fungicide-resistant strains emphasize the need for sustainable disease
105 management strategies beyond conventional breeding and chemical approaches. To better
106 understand the molecular basis of disease suppression, previous studies have primary focused
107 on the *C. fulvum*–tomato interaction within the framework of the gene-for-gene model, but
108 tripartite interactions involving additional microorganisms remain largely unexplored.
109 *Hansfordia pulvinata* (Berk. & M.A. Curtis) S. Hughes (syn. *Dicyma pulvinata*) is a
110 mycoparasitic fungus serendipitously discovered on tomato leaves infected with *C. fulvum* in
111 a greenhouse (Iida *et al*., 2018). It overgrows *C. fulvum* lesions on the plant host, effectively
112 suppressing disease progression, and has broad mycoparasitic activity against all known *C.*
113 *fulvum* races (Iida *et al*., 2018). *H. pulvinata* recognizes *C. fulvum* hyphae, coils around them,
114 and directly penetrates the hyphae, then forms intercellular structures within the host fungus
115 (Peresse & Le Picard, 1980; Maeda *et al*., 2025). It also produces an eremophilane-type
116 sesquiterpenoid, 13-deoxyphomenone (also known as sporogen-AO1), which has antifungal
117 activity against *C. fulvum* (Tirilly *et al*., 1983; Maeda *et al*., 2025). The compound was
118 initially identified as a sporulation-inducing factor in the koji mold *Aspergillus oryzae*
119 (Tanaka *et al*., 1984a, 1984b). Comparative genomics recently revealed that the biosynthetic
120 gene cluster for 13-deoxyphomenone (*DPH*) in *H. pulvinata* shares high synteny with that in
121 *Aspergillus* species, suggesting horizontal gene transfer from an ancestoral *Aspergillus*
122 lineage (Maeda *et al*., 2025). Subsequently, *H. pulvinata* appears to have retained this
123 gene cluster to support its mycoparasitic lifestyle, repurposing the endogenic sporogenesis
124 function in *Aspergillus* species into exogenic antifungal activity that inhibits spore
125 germination and hyphal elongation of *C. fulvum*. However, the molecular mechanisms
126 underlying its mycoparasitism remain largely unknown. Since its mycoparasitism is not
127 restricted to the phyllosphere (Maeda *et al*., 2025), comparative analyses of fungal–fungal
128 interactions under different mycoparasitic conditions could provide new insights on the
129 molecular basis of fungal host recognition and leaf-surface biocontrol mechanisms.
130 The *C. fulvum*–tomato interaction has long served as a valuable model for dissecting
131 gene-for-gene dynamics in plant–pathogen systems (Mesarich et al. 2023.). Recent
132 chromosome-scale genome assemblies of multiple *C. fulvum* races have substantially
133 advanced our understanding of its genome structure and effector repertoire (Zaccaron *et al*.,
134 2022; Zaccaron & Stergiopoulos, 2024). Nevertheless, the molecular basis governing fungal–

135 fungal recognition and the tripartite interactions with tomato plants remain largely
136 uncharacterized. Here, we present transcriptomic evidence revealing how the mycoparasitic
137 fungus *H. pulvinata* modulates both *C. fulvum* and tomato responses, providing molecular
138 insights into the interplay among plant, pathogen and mycoparasite. These findings
139 underscore the potential of the foliar mycoparasitic fungus as promising biocontrol agents
140 within complex plant–microbe ecosystems.
141

142 **MATERIALS AND METHODS**

143 **Culture conditions for fungal strains and plants, treatments and assays**

144 Fungal strains *H. pulvinata* 414-3 and *C. fulvum* CF301 were cultured on half-strength potato
145 dextrose agar (PDA; BD Difco, Sparks, MD, USA) or minimal medium (MM) agar (15 g
146 sucrose, 5 g ammonium tartrate, 1 g NH_4NO_3, 1 g KH_2PO_4, 0.5 g $MgSO_4 \cdot 7H_2O$, 0.1 g NaCl,
147 0.1 g $CaCl_2 \cdot H_2O$, 25 µL 0.2 mg mL^{-1} biotin, 15 g agar and 1 mL trace elements per liter) at
148 25 °C in the dark for 1 (*H. pulvinata*) and 2 weeks (*C. fulvum*) (Maeda *et al*., 2025). Spores
149 were collected in distilled water and adjusted to 1×10^6 spores mL^{-1} using a hemocytometer.
150 For *in vitro* assays, 100 µL of one of the spore suspensions was spread onto nylon
151 membranes on PDA and incubated for 1 week for *H. pulvinata* (hereafter "*in vitro Hp*") or 2
152 weeks for *C. fulvum* ("*in vitro Cf*") (Fig. **S1a**). For set up the *in vitro* mycoparasitic intection,
153 membranes bearing *C. fulvum* colonies were transferred to water agar (nutrient-poor) and
154 sprayed with 1 mL of *H. pulvinata* spore suspension (1×10^6 spores mL^{-1}); plates were then
155 incubated at 25 °C in the dark for 2 weeks ("*in vitro Cf/Hp*") (Fig. **S1a**).

156 Seedlings of tomato (*Solanum lycopersicum*) cv. Moneymaker (lacking all known *Cf*
157 resistance genes) were grown at 25 °C with 16 h light/8 h dark. Four-week-old plants were
158 either grown in high humidity as healthy controls for another 2 weeks (healthy leaf; Fig. **S1a**)
159 or sprayed with approximately 3 mL of a *C. fulvum* spore suspension (1×10^6 spores mL^{-1}),
160 then incubated in high humidity for 2 weeks until lesions developed ("*in planta Cf*"
161 interaction; Fig. **S1a**). For establishing the mycoparasitism in plants, plants with leaf mold
162 lesions were sprayed with approximately 3 mL of *H. pulvinata* spore suspension (1×10^6
163 conidia mL^{-1}) and incubated under high humidity at 25 °C for 2 weeks until lesions were
164 overgrown by white mycelia of *H. pulvinata* ("*in planta Cf/Hp*"; Fig. **S1a**).

165 *N. benthamiana* plants were grown for 4 weeks at 25 °C with 16 h light/8 h dark.
166 *Arabidopsis thaliana* ecotype Col-0 seeds were surface-sterilized in 70% (v/v) ethanol for 1
167 min, rinsed three times with sterile distilled water, plated on Murashige and Skoog (MS) agar

168 (4.33 g MS basal medium (Sigma-Aldrich, St. Louis, MO, USA) and 20 g sucrose per liter,
169 pH 5.7), stratified at 4 °C in the dark for 1 month, then transferred to soil and grown for 5
170 weeks at 25 °C with 16 h light/8 h dark.
171
172 **Scanning electron microscopy (SEM)**
173 Sample preparation and imaging procedures for SEM were described previously (Maeda *et*
174 *al*., 2025). Nylon membranes with fungal cultures were cut into squares with sides of about 5
175 mm and fixed in 2.5% (v/v) glutaraldehyde in 100 mM cacodylate buffer (pH 7.4) overnight
176 at 4 °C, then 1% (w/v) osmium tetroxide in 100 mM cacodylate buffer (pH 7.4) for 1 h at
177 room temperature. Samples were then dehydrated with a graded ethanol series, critical-point
178 dried in absolute ethanol using a Leica EM CPD300 critical point dryer (Leica Microsystems,
179 Wetzlar, Germany), then mounted on stubs, coated with platinum-palladium, and observed
180 with a Hitachi SU-8220 scanning electron microscope (Tokyo, Japan).
181
182 **RNAseq and transcriptome analysis**
183 Three biological replicates were collected from the fungal colonies on membranes or from
184 leaves for each treatment described above. Total RNA was extracted using the RNeasy Plant
185 Mini Kit (Qiagen, Hilden, Germany) according to the manufacturer's instructions. Poly(A)
186 mRNA was enriched with the NEBNext Poly(A) mRNA Magnetic Isolation Module (New
187 England Biolabs, Ipswich, MA, USA), and libraries were prepared using the NEBNext Ultra
188 II Directional RNA Library Prep Kit (New England Biolabs). Libraries were sequenced on an
189 Illumina NovaSeq 6000 platform (Illumina, San Diego, CA, USA) with the PE150 kit (150
190 bp × 2 paired-end), producing 2 or 4 Gb of data per sample.
191 Raw read quality was assessed using FastQC Ver. 16.0.1
192 (bioinformatics.babraham.ac.uk/projects/fastqc). Low-quality bases and adapter sequences
193 were removed using Trimmomatic Ver. 0.39 (Bolger *et al*., 2014). Clean reads were aligned
194 to the respective reference genomes using HISAT2 Ver. 2.2.1; SAM files were converted to
195 BAM files with SamTools Ver. 1.18 (Li *et al*., 2009; Kim *et al*., 2019). Read counts were
196 generated using Rsubread Ver. 2.20.0. Differentially expressed genes (DEGs) were identified
197 with DESeq2 using thresholds of $|\log_2 \text{Fold-change}| \geq 1$ and adjusted *P*-value (padj) ≤ 0.05
198 (Love *et al*., 2014). Gene Ontology (GO) and KEGG enrichment analyses were performed
199 using TBtools-II Ver. 2.119 (Aleksander *et al*., 2023; Chen *et al*., 2023; Kanehisa *et al*.,
200 2025). Data were visualized using SRplot (Tang *et al*., 2023).
201

202 **Bioinformatic analysis**

203 Orthologous coding sequences were identified using OrthoFinder Ver. 2.5.5 (Emms & Kelly,
204 2019); 100 single-copy orthologs were selected for multiple sequence alignment. Sequence
205 alignments were generated using MAFFT Ver. 7.526 and subsequently trimmed with TrimAl
206 Ver. 1.4 (Katoh and Standley, 2013; Capella-Gutiérrez *et al*., 2009). Maximum-likelihood
207 phylogenetic trees were constructed with RAxML Ver. 8.2.12 using 1,000 bootstrap
208 replicates and the GTRCAT or PROTCATAUTO model (Stamatakis, 2014). The consistency
209 of the tree topology was assessed using approximately unbiased (AU) tests (Shimodaira,
210 2002) with 10,000 bootstrap replicates as previously described (Maeda *et al*., 2025). Signal
211 peptides were predicted with SignalP-6.0 (Teufel *et al*., 2022), candidate effectors with
212 EffectorP-fungi 3.0 (Sperschneider & Dodds, 2022), and subcellular localization with
213 LOCALIZER (Sperschneider *et al*., 2017). Secondary metabolite biosynthetic gene
214 clusters were identified using the fungal version of antiSMASH (Blin *et al*., 2023). GPI-
215 anchored proteins were predicted with NetGPI 1.1 (Gíslason *et al*., 2021), and carbohydrate-
216 active enzymes (CAZymes) were annotated using DIAMOND (Zhang *et al*., 2018). Default
217 parameters were used for all analyses unless otherwise specified.

218 For sequence similarity comparison, the EMBOSS Needle tool was used for pairwise
219 alignments (Madeira *et al*., 2024). Protein domains and motifs were predicted using the
220 Pfam database and the MEME Suite, respectively (Bailey *et al*., 2015; Mistry *et al*., 2021).
221 The 3D structures of proteins were predicted using ColabFold Ver. 1.5.5) (Mirdita *et al*.,
222 2022). Five models were generated with three iterative recycles each, and the models were
223 ranked according to their predicted local distance difference test (pLDDT) scores. The top-
224 ranked models were refined by AMBER energy minimization to resolve steric clashes and
225 improve stereochemical geometry. The resulting relaxed structures were used for subsequent
226 structural analyses. The structure of Ecp2 was analyzed using the Dali server to retrieve
227 structural homologs based on a non-redundant data set clustered at 25% sequence identity
228 (PDB25), and structures were compared with TM-align (Zhang & Skolnick, 2005; Holm,
229 2022).

230

231 **Plasmid construction and protein expression**

232 NLP coding sequences were synthesized (VectorBuilder, IL, USA) and cloned into the
233 pSfinx vector using a primer set (Table **S1**) and NEBuilder HiFi assembly kit (New England
234 Biolabs). The NLP genes were digested with restriction enzyme EcoRI and subcloned into
235 the pPIC9K vector (Thermo Fisher Scientific, Waltham, MA, USA) for expression in *Pichia*

236 *pastoris* GS115 strain according to the manufacturer's instructions. Transformants were
237 selected on YPD medium (Fujifilm Wako, Osaka, Japan) containing G418 (Fujifilm Wako)
238 and confirmed by PCR using the primer set in Table **S1**. Expression was induced by adding
239 5 mL of the pre-culture grown in BMGY broth to 100 mL of BMMY supplemented with
240 1.5% (w/v) methanol, and incubating the culture at 30 °C and 300 rpm for 96 h. Supernatants
241 were collected by centrifugation at 12,000 rpm for 10 min.
242 The gene *Ecp2* was amplified from genomic DNA of *C. fulvum* using PCR and the
243 primer set in Table **S1** and cloned into the pET-28b vector (Merck, Darmstadt, Germany) to
244 express an N-terminal His_6-tagged protein in *Escherichia coli* strain BL21(DE3). Expression
245 was induced in LB medium with 1 mM IPTG at 16 °C for 16 h. Cells were resuspended with
246 50 mM KPi buffer (pH 7.4) and disrupted by sonication on ice (10 min: 2 s on–4 s off).
247 Insoluble fractions were solubilized in 10 mL of denaturing buffer (6 M guanidine
248 hydrochloride, 10 mM Tris, 10 mM β-mercaptoethanol, pH 8.0) for 1 h at room temperature.
249 Proteins were purified in a Ni-affinity column HisTrap HP (Cytiva, Medemblik, The
250 Netherlands), concentrated using Vivaspin 6 (GE Healthcare, Chicago, IL, USA) and
251 quantified with a Qubit fluorometer (Thermo Fisher Scientific). BL21(DE3) carrying empty
252 pET-28b served as a negative control.
253
254 **Western blot analysis**
255 All protein samples were heated at 95 °C for 10 min in sample buffer (1% SDS, 1% 2-
256 mercaptoethanol, 10 mM Tris–HCl, 20% (v/v) glycerol, pH 6.8) for denaturation. The
257 proteins were separated in 12% SDS-polyacrylamide gel and transferred onto PVDF
258 membrane (Bio-Rad, Hercules, CA, USA). Membranes were blocked with 5% skim milk in
259 TBS-T for 1 h before antibody incubation. Anti-His and anti-HA monoclonal antibodies (Cell
260 Signaling Technology, Danvers, MA, USA) were diluted in Can Get Signal solution 1
261 (1:10,000) (TOYOBO, Osaka, Japan) and used as primary antibodies to detect Ecp2 and
262 NLPs, respectively. Horseradish peroxidase-conjugated anti-rabbit antibody was diluted with
263 Can Get Signal solution 2 (1:2,000) (TOYOBO) for use as the secondary antibody. Signals
264 were visualized using an ECL western detection kit (GE Healthcare) and captured using a
265 ChemiDoc imaging system (Bio-Rad).
266
267 **Functional assay of NLPs**
268 pSfinx plasmids were introduced into *Agrobacterium tumefaciens* strain GV3101 via
269 electroporation (Ma *et al*., 2012). Agrobacterium suspensions were adjusted to OD_{600} = 0.3 in

infiltration buffer (2.03 g $MgCl_2 \cdot 6H_2O$, 1.95 g MES, 500 μL of 200 mM acetosyringone per liter, pH 5.6) and used to infiltrate leaves on 4-week-old plants of *N. benthamiana* by syringe pressure. Leaves were monitored for necrosis 14 days after infiltration. Necrosis was visualized by trypan blue staining (Ma *et al*., 2012) and quantified using ilastik (Ver. 1.4.1) (Berg *et al*., 2019).

P. pastoris culture supernatant containing NLP proteins or BM medium (BMGY without glycerol) was mixed at a 1:1 ratio with *C. fulvum* spore suspension (1×10^6 spores mL^{-1}). A 40 μL drop of each mixture was placed on a hydrophobic glass slide and incubated at room temperature for 24 h. After incubation, germination of 200 spores per treatment was assessed using a Nikon E600 light microscope (Tokyo, Japan). Culture supernatants containing NLP proteins were collected from *P. pastris* and used to syringe-infiltrate *N. benthamiana* leaves. Twenty-four hours after infiltration, apoplastic fluid was collected by vacuum infiltration with distilled water, followed by centrifugation (1,000 rpm, 10 min) (Joosten, 2012). Equal volumes (10 μL) of *C. fulvum* spore suspension and apoplast fluid were then incubated at room temperature for 24 h. A light microscope (Nikon) was then used to assess 200 spores for germination.

Synthetic peptides of nlp24 (GenScript Biotech, Nanjing, China) were prepared in 500 nM stock solutions in dimethyl sulfoxide. Reactive oxygen species (ROS) were detected as previously described with slight modifications (Yang *et al*., 2022). Leaf disks (0.125 cm^2) of *N. benthamiana* were floated on sterile distilled water for 24 h, then treated with 10 μL of a substrate mixture (5 μL of 10 mM L-012 [Fujifilm Wako] and 5 μL of protein or peptide). Luminescence was recorded every 2 min for 40 min using a Tristar3 Multimode Reader (Berthold Technologies, Bad Wildbad, Germany).

Functional assays of Ecp2

The abaxial side of *Cf-ECP2* tomato leaves was infiltrated with purified Ecp2 protein (final concentration 1 μM) using a syringe. Leaves were incubated at 25 °C with 16 h light/8 h dark for 6 d and checked for a hypersensitive response (HR). *In vitro* antifungal activity was assayed as previously described (Chavarro-Carrero *et al*., 2024). Briefly, fungal spores were suspended in 5% PDB containing 15 μM Ecp2 or empty vector control (1×10^4 spores mL^{-1}), then 100 μL of the samples (three wells per sample) was incubated in wells of 96-well plates at 25 °C for 4 days. For each well, five fields of view were photographed ($N = 15$). Fungal growth was quantified and compared with the control using the Hybrid Cell Count module of

303 the BZ-800X (KEYENCE, Osaka, Japan).
304
305 **Statistical analyses**
306 R version 4.4.2 (R Core Team, 2024) was used for all analyses. The proportion of necrosis
307 relative to total leaf area in *N. benthamiana* was assessed using Dunnett's test, with the empty
308 vector as the control ($N = 3$). Spore germination rate of *C. fulvum* treated with NLPs was
309 analyzed by one-way ANOVA followed by Tukey's HSD test ($N = 3$). The spore germination
310 rate of *C. fulvum* in apoplastic fluid from *N. benthamiana* leaves treated with NLPs was
311 compared using the Mann–Whitney U test, with the buffer as the control ($N = 12$). The
312 relative growth rate of fungi and yeast treated with Ecp2 was compared using Student's t-test,
313 with the empty vector as the control ($N = 15$).
314
315 **RESULTS**
316 **Overview of RNA-seq data sets**
317 RNA was extracted from healthy control leaves, leaves infected with *C. fulvum* (*in planta*
318 *Cf*), and leaves with *C. fulvum* lesions overgrown by *H. pulvinata* (*in planta Cf/Hp*) (Fig. **1a**;
319 Fig. **S1a**). Because *H. pulvinata* parasitizes *C. fulvum* in leaf and on nutrient-poor water agar
320 (Iida *et al*., 2018; Maeda *et al*., 2025), fungal RNA was also extracted from *in vitro* cultures
321 of *H. pulvinata* alone (*in vitro Hp*), *C. fulvum* alone (*in vitro Cf*), and dual cultures of *C.*
322 *fulvum* and *H. pulvinata* (*in vitro Cf/Hp*) on water agar (Fig. **1a**; Fig. **S1a**). Typical white
323 mycelium of the mycoparasite *H. pulvinata* was observed at 14 days after inoculation for the
324 *in planta Cf/Hp* and *in vitro Cf/Hp* interactions (Fig. **1a**). Microscopic observation confirmed
325 that *H. pulvinata* penetrated *C. fulvum* hyphae (Fig. **1b**) and that *C. fulvum* entered tomato
326 leaves through stomata (Fig. **S1b**) as previously described (Maeda *et al*., 2025). Also, hyphae
327 of *H. pulvinata* elongated on the leaf surface and entered stomata in the presence of *C. fulvum*
328 (Fig. **S1b**). Raw reads were aligned to the reference genome sequences of *H. pulvinata*, *C.*
329 *fulvum* and tomato plants using HISAT2. The proportion of uniquely mapped reads varied
330 across samples, ranging from 10.3% and 88.1% (Table **S2**), reflecting the multiorganismal
331 nature of several samples. Principal component analysis (PCA) of normalized expression
332 values revealed clear clustering of biological replicates by treatment for each organism,
333 indicating high within-treatment reproducibility (Fig. **S1c**). In the transcriptome analysis, we
334 identified DEGs using adjusted P-value (padj) ≤ 0.05 and $|\log_2 \text{Fold-change}| \geq 1.0$. Functional
335 enrichment of DEGs was performed using KEGG pathway annotation to reveal biological
336 processes that are positively and negatively regulated during mycoparasitism.

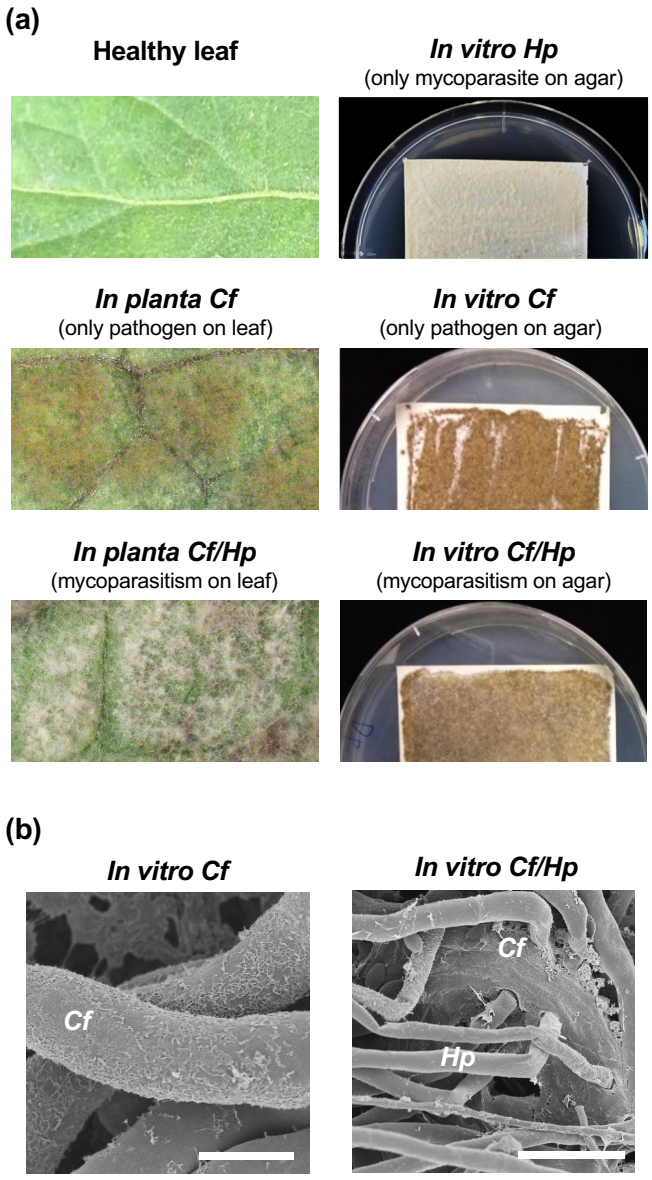

Fig. 1. *Cladosporium fulvum* parasitized by mycoparasitic fungus *Hansfordia pulvinata*. (a) Typical healthy tomato leaf, lesions caused by *C. fulvum* (*in planta Cf*), and lesions covered by white mycelium of *H. pulvinata* (*in planta Cf/Hp*). Tomato plants had lesions by 2 weeks after inoculation with *C. fulvum*. The diseased leaves were then inoculated with *H. pulvinata*, and after 1 week, white mycelia were observed on lesions. *In vitro* cultures: *H. pulvinata* (*in vitro Hp*) and *C. fulvum* (*in vitro Cf*) were grown on nylon membranes on water agar after transfer from PDA. *H. pulvinata* parasitized *C. fulvum* colonies on water agar (*in vitro Cf/Hp*). (b) Scanning electron micrographs of hyphae of *C. fulvum* and *H. pulvinata* in the *in vitro Cf* and *Cf/Hp* interactions. *H. pulvinata* hyphae have penetrated *C. fulvum* hyphae. Bar indicates 10 μm.

Transcriptomic reprogramming in *H. pulvinata* after its parasitism of *C. fulvum*

Transcriptome analysis of RNA from the mycoparasitic interactions (*in vitro Cf/Hp* and *in planta Cf/Hp*) and the control (*in vitro Hp*) was used to identify DEGs involved in mycoparasitism based on gene annotations (Table **S3**). During the *in vitro Cf/Hp* interaction, 1,336 genes were significantly upregulated and 738 genes downregulated (Fig. **2a**), compared with 1,793 upregulated and 2,086 downregulated during mycoparasitism on the plant (*in planta Cf/Hp*). The DEGs in these two mycoparasitic interactions shared a core set of 891 upregulated and 557 downregulated genes and mapped to 21 upregulated and 25

371 downregulated KEGG pathways (Fig. **2b**), suggesting that *H. pulvinata* activated a conserved
372 transcriptional program during mycoparasitism, whether it occurs *in vitro* or *in planta*
373 environments.

374 The KEGG pathways that were enriched in *H. pulvinata* during mycoparasitism imply
375 both primary and secondary metabolism were reprogrammed. KEGG pathways involved in
376 secondary metabolism, including steroids, terpenoids, and polyketides, were strongly
377 upregulated. Genome mining prediction revealed 33 putative biosynthetic gene clusters for
378 secondary metabolites in *H. pulvinata*—12 non-ribosomal peptide synthetases (NRPSs), 10
379 type I polyketide synthases (T1PKSs), 7 terpenes, 3 fungal ribosomally synthesized and post-
380 translationally modified peptides (fungal-RiPPs), and an isocyanide—all of which underwent
381 a marked transcriptional change during mycoparasitism (Table **S4**). Deoxyphomenone
382 biosynthesis (*DPH*) genes were also upregulated, consistent with *H. pulvinata* producing the
383 antifungal sesquiterpenoid 13-deoxyphomenone during mycoparasitism (Table **S4**) (Tirilly *et*
384 *al*., 1983; Maeda *et al*., 2025). Interestingly, multiple amino acid metabolism pathways were
385 consistently downregulated, despite *H. pulvinata* growing vegetatively during
386 mycoparasitism (Fig. **2b**). Given the central role of amino acids for protein synthesis and
387 vegetative growth, this KEGG pattern suggested that *H. pulvinata* may acquire amino acids
388 derived from *C. fulvum* or tomato plants to supplement its amino acid pool during
389 mycoparasitism.

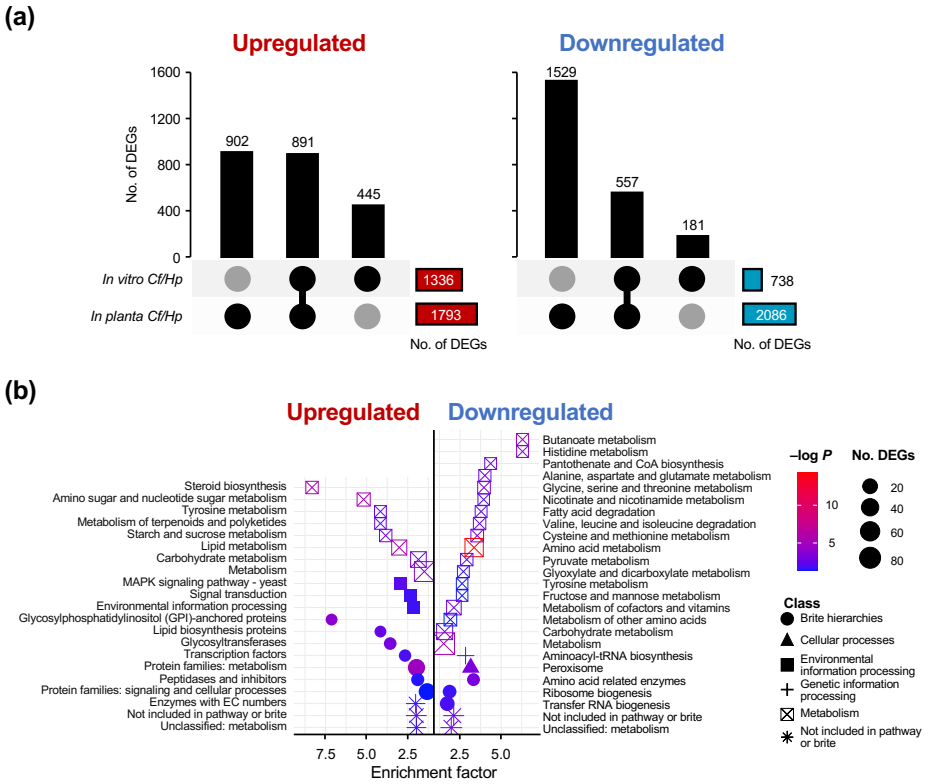

390

391 **Fig. 2. Differentially expressed genes (DEGs) and enriched KEGG pathways in**
392 ***Hansfordia pulvinata* during its parasitism of *Cladosporium fulvum*.** (a) UpSet plot of
393 DEGs in *in vitro* and in tomato (*in vitro Cf/Hp* and *in planta Cf/Hp*; Fig. 1a). Connected dots
394 indicate shared DEGs; black single dots represent condition-specific DEGs. Vertical bars
395 show the number of up- and downregulated genes; colored horizontal bars indicate the total
396 number of DEGs detected in each interaction. (b) Bubble plot of KEGG pathway enrichment
397 analysis of the 891 and 557 shared DEGs shown in (a). Keys: color of symbols indicates
398 significance level of enrichment (–log adjusted *P*); size of symbol indicates the number of
399 enriched DEGs in each pathway; the symbol indicates the functional class of the enriched
400 DEGs.
401
402
403 **Expression profile and functional analysis of small secreted proteins in *H. pulvinata***
404 A comparison of the genome structures of *H. pulvinata* with those of fungi including plant
405 pathogens and mycoparasite *Trichoderma atroviride* revealed that *H. pulvinata* had the
406 fewest genes encoding carbohydrate-active enzymes (CAZymes), but the most genes
407 containing the signal peptide sequence for secretion (Fig. **S3**; Table **S3**). To analyze the
408 secretome, we filtered 891 DEGs commonly upregulated in both mycoparasitic interactions
409 (*in vitro Cf/Hp* and *in planta Cf/Hp*) and identified 165 genes encoding small secreted
410 proteins (Fig. **3a**). Although most of them could not be annotated for function, 27 were
411 annotated as genes previously reported to be associated with pathogenicity in plant
412 pathogenic fungi, including glycoside hydrolase, T2 family ribonuclease, EPL1-like protein
413 (orthologous to Ecp45 effector protein in *C. fulvum*), hydrophobin, necrosis-inducing protein,
414 KP4-type killer toxin proteins, cutinase-like protein, superoxide dismutase protein,
415 endoglucanase, and metalloprotease (Table **S5**). We focused on a necrosis-inducing protein
416 (DIP_10004627), designated *HpNLP1*, which is an Nep1-like protein (NLP) homologous to
417 PsojNIP because *HpNLP1* showed particularly high $-\log_{10}$ *P*-adj, indicating a high level of
418 significance (Fig. **3b**; Fig. **S4**). NLPs represent a widespread family of virulence-associated
419 proteins in plant pathogens that trigger necrosis and generation of ROS in host plants (Seidl
420 & Van den Ackerveken, 2019). Expression of *HpNLP1* increased 34-fold during the
421 mycoparasitism *in vitro* and 14-fold *in planta* (Table **S5**). The NLP gene *HpNLP2*
422 (DIP_10008029) was also present in *H. pulvinata*, but its expression was unchanged during
423 mycoparasitism.
424

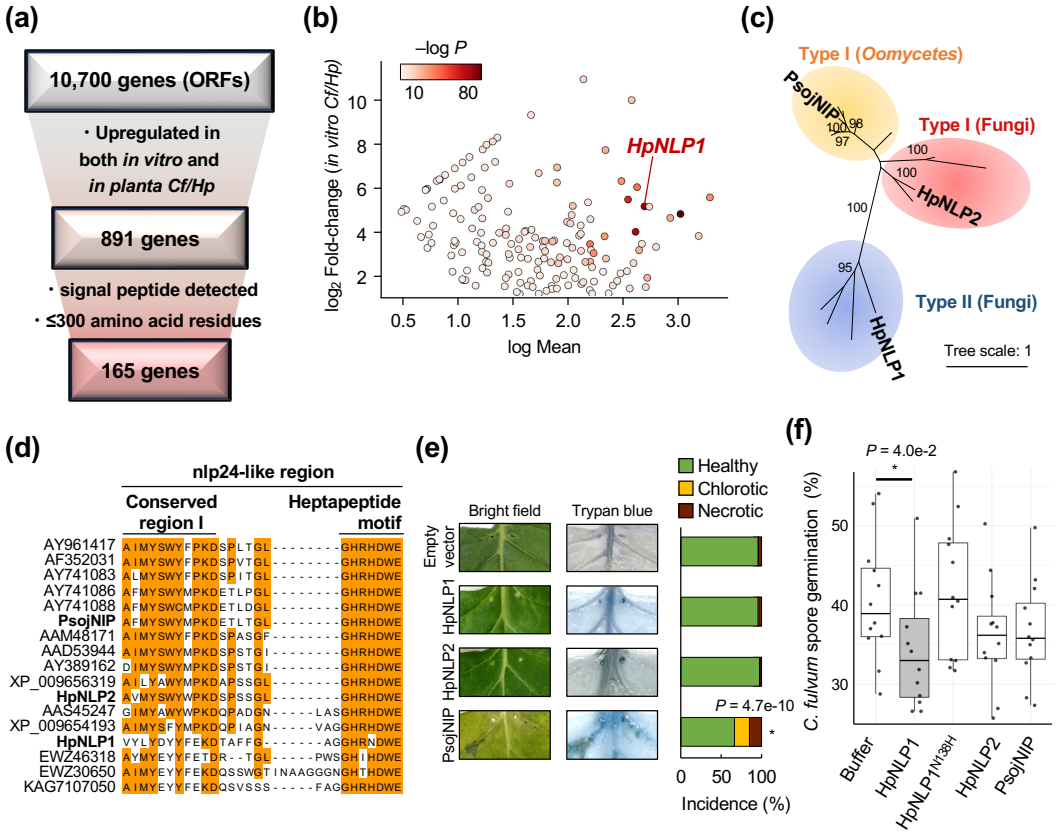

Fig. 3. A Nep1-like protein (NLP) secreted from the mycoparasite *Hansfordia pulvinata* induces a plant-mediated toxicity against spores of *Cladosporium fulvum*. (a) Workflow for identifying small secreted proteins synthesized in *H. pulvinata* during mycoparasitism. (b) MA plot for expression levels of 165 selected genes. Cutoff thresholds are $\log_2$ Fold-change (±1.0) for *in vitro Cf/Hp* interaction and log Mean (0.3). (c) Phylogenetic tree based on NLP amino acid sequences using the maximum likelihood method with 1,000 bootstrap replicates. Protein accession numbers are shown in (d). Type I and Type II have two and four cysteine residues, respectively. Proteins analyzed in this study are in bold. (d) Multiple sequence alignment of NLP using MAFFT. Conserved residues are highlighted in orange. (e) Transient expression assays of NLPs in *Nicotiana benthamiana* via agroinfiltration. Chlorosis and necrosis were assessed 14 days after infiltration by trypan blue staining. Similar results were obtained in three independent experiments; representative results are in Supplementary Fig. S5c. (f) Percentage germination of conidia of *C. fulvum* after 24-h treatment with apoplastic fluid from *N. benthamiana* leaves that had been infiltrated with different NLPs or buffer. Asterisks indicate significant differences between treatments determined using Dunnett's or the Mann–Whitney *U* test.

444 Phylogenetic analysis placed HpNlp1 and HpNlp2 within the type II and fungal type I
445 clades (Seidl and van den Ackerveken, 2019), respectively, in NLPs (Fig. **3c**). HpNlp1
446 contained four cysteine residues predicted to form two disulfide bonds between positions 39–
447 65 and 82–87 (Fig. **S4a** and **b**). Multiple sequence alignment showed that both HpNlp1 and
448 HpNlp2 contained the conserved region I and the C-terminal heptapeptide GHRHDWE
449 motif; this conserved 24-amino-acid peptide (nlp24) is recognized as a microbe- or pathogen-
450 associated molecular pattern (MAMP/PAMP) (Oome *et al*., 2014). The tryptophan (W) and
451 proline (P) residues essential for necrosis-inducing activity in the conserved region I (Zhou *et*
452 *al*., 2012) were conserved in HpNlp2 but replaced by tyrosine (Y) and glutamic acid (E) in
453 HpNlp1 (Fig. **3d**), which was the only NLP strongly expressed during mycoparasitism. In the
454 heptapeptide motif of HpNlp1, the second histidine (H) was replaced by asparagine (N) (Fig.
455 **3d**). Structural superposition of PsojNIP and HpNlp1 yielded a TM-score of 0.86 and a root
456 mean square deviation (RMSD) of 1.93 Å, demonstrating that despite mutations in the nlp24-
457 like regions of HpNlp1, the global protein structure was largely preserved, as indicated by the
458 similar these values compared to the PsojNIP (Fig. **S4c**).
459 Recombinant proteins PsojNIP, HpNlp1 and HpNlp2 were produced in *P. pastoris* and
460 used to infiltrate *Nicotiana benthamiana* leaves. Western blot analysis of HpNlp1
461 demonstrated an additional band larger than the predicted molecular weight, suggesting dimer
462 formation (Fig. **S5a** and **b**). As previously reported, PsojNIP induced necrosis and chlorosis
463 (Qutob *et al*., 2002), whereas HpNlp1 and HpNlp2 did not trigger visible necrosis or ROS
464 accumulation (Fig. **3e**; Fig. **S5c** and **d**). The high expression of *HpNLP1* gene during the
465 bipartite *in vitro Cf/Hp* interaction, in the absence of the plant, suggested that HpNlp1 might
466 directly suppress *C. fulvum* growth. Contrary to this expectation, no such direct antifungal
467 activity was detected against *C. fulvum* spore germination and hyphal elongation (Fig. **S5e**).
468 Remarkably, however, fluid from the apoplast—where *C. fulvum* grows—collected from *N.*
469 *benthamiana* leaves that had been infiltrated with HpNlp1 strongly suppressed *C. fulvum*
470 spore germination, whereas the protein with a point mutant ($HpNlp1^{N138H}$) failed to elicit
471 antifungal activity (Fig. **3f**). Neither of the nlp24 peptides of HpNlp1 and $HpNlp1^{N138H}$
472 induced RLP23-mediated resistance (Fig. **S5f**). These findings together demonstrated that
473 HpNlp1 diverges from typical necrosis-inducing NLPs in plant pathogens, inducing the
474 accumulation of apoplastic antifungal substances that suppress *C. fulvum* spore germination
475 instead of promoting host cell death.
476
477 **Transcriptomic responses of pathogen *C. fulvum* parasitized by *H. pulvinata***

Next, we investigated the DEGs of *C. fulvum* through KEGG pathway analysis after tomato was infected by *C. fulvum* (*in planta Cf*), dual infection in tomato leaves (*in planta Cf/Hp*), and dual culture on agar (*in vitro Cf/Hp*) (Fig. **1a**). DEGs in *C. fulvum* were identified relative to the *in vitro Cf* control on water agar. A total of 1,902 genes were upregulated and 1,783 genes were downregulated when *C. fulvum* infected tomato leaves (*in planta Cf*) (Fig. **4a**). In the two mycoparasitic interactions, 2,195 upregulated and 2,435 downregulated genes were detected *in planta Cf/Hp*, and 1,479 upregulated and 845 downregulated were *in vitro Cf/Hp*. We identified 363 upregulated and 158 downregulated genes shared between the two mycoparasitic interactions (*in vitro Cf/Hp* and *in planta Cf/Hp*), indicating a conserved transcriptional response to *H. pulvinata* attack. KEGG enrichment analysis assigned these shared DEGs to seven upregulated and three downregulated pathways, revealing strong activation of protein folding and processing pathways in *C. fulvum* upon mycoparasitism by *H. pulvinata* (Fig. **4b**). Conversely, genes involved in amino acid metabolism were consistently downregulated, as also observed for *H. pulvinata*, suggesting coordinated suppression of primary metabilisms in this fungal–fungal interaction.

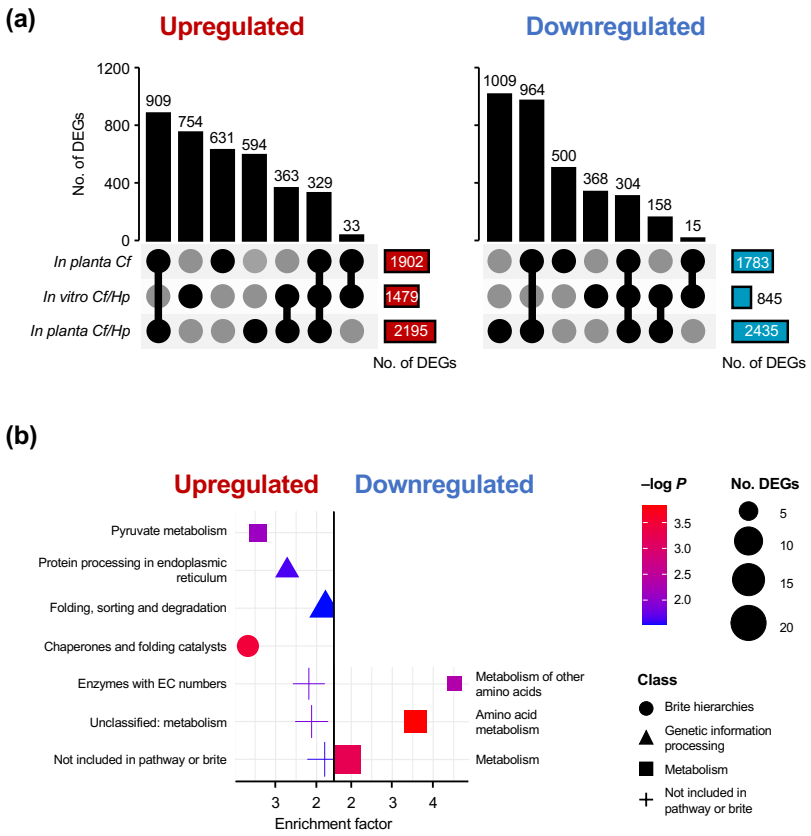

Fig. 4. Differentially expressed genes (DEGs) and enriched KEGG pathways in phytopathogen *Cladosporium fulvum*. (a) UpSet plot showing DEGs identified in the *in*

496 *planta Cf*, *in vitro Cf/Hp*, and *in planta Cf/HP* interactions (see Fig. 1A). Connected dots
497 indicate shared DEGs; Black single dots represent condition-specific DEGs. Vertical bars
498 show the numbers of up- and downregulated genes; colored horizontal bars indicate the total
499 number of DEGs detected in each interaction. (b) Bubble plot of KEGG pathway enrichment
500 analysis based on the 363 and 158 shared DEGs shown in (a). Keys: color of symbols
501 indicates significant level of enrichment (–log adjusted *P*); size of symbol indicates the
502 number of enriched DEGs in each pathway; the symbol indicates the functional class of the
503 enriched DEGs.
504
505
506 In *C. fulvum*, protein folding and processing pathways were strongly activated when
507 parasitized by *H. pulvinata* (Fig. **4a**). These responses are indicative of ER stress and
508 accumulation of misfolded proteins, phenomena often triggered by exposure to antifungal
509 compounds (Chaillot *et al*., 2015). Similar to the results in the mycoparasite *H. pulvinata*, the
510 downregulation of secondary metabolism-related genes suggested that *C. fulvum* reallocated
511 resources from the production of secondary metabolites to survive and mitigate stress. The
512 expression profiles of DEGs detected in *C. fulvum* were further analyzed based on functional
513 classification previously reported by Zaccaron & Stergiopoulos (2024). Among the 42 genes
514 associated with secondary metabolite biosynthesis, 15 (35.7%) and 18 (42.8%) were
515 downregulated in the *in planta Cf* and *in planta Cf/Hp* interactions, respectively (Fig. **5a**;
516 Table **S6**). Thirteen genes, including *PKS6* (CLAFUR5_12905), a key enzyme in cladofulvin
517 biosynthesis (Griffiths *et al*., 2018), were consistently downregulated in both interactions.
518 In contrast, the category small secreted proteins had the most upregulated DEGs,
519 including numerous known or predicted effectors (Fig. **5a**). An expression heatmap of
520 effector genes showed that, as expected, the majority of the 106 effector genes were highly
521 expressed when *C. fulvum* infected leaves in the *in planta Cf* interaction (Fig. **5b**). Expression
522 of effector genes are generally silent on synthetic media (Mesarich *et al*., 2014); however,
523 surprisingly, 56 effector genes were upregulated in the *in vitro* coculture of *C. fulvum* and *H.*
524 *pulvinata* (*in vitro Cf/Hp*) (Fig. **5b**). In tomato leaves, effector expression in *C. fulvum*
525 remained high regardless of the presence of *H. pulvinata* (Fig. **S6**). These results suggested
526 that *C. fulvum* effectors may play a defensive role, acting as countermeasures against
527 mycoparasitic attack by *H. pulvinata.* To investigate this possibility, we conducted an
528 AMAPEC analysis, which predicts antimicrobial proteins based on 3D-structural signatures
529 (Mesny *et al*., 2024). Of the 56 effector genes that were upregulated during the *in vitro Cf/Hp*

530 interaction, 34 were predicted to possess antimicrobial activity, suggesting that many
531 effectors may act as antifungal proteins (Fig. **5c**; Table **S7**). Among these, we focused on the
532 effector Ecp2, which is known to trigger a hypersensitive response (HR) in tomato cultivars
533 carrying the *Cf-ECP2* resistance gene.

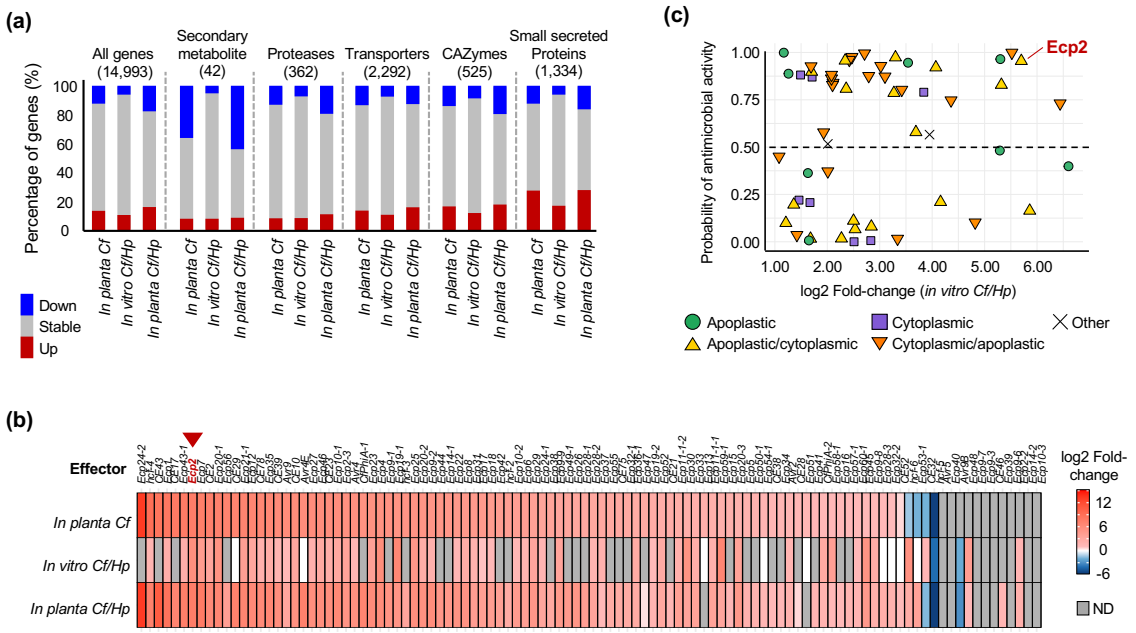

534

535 **Fig. 5. Effector genes in phytopathogen *Cladosporium fulvum* were highly expressed**
536 **during mycoparasitism by *Hansfordia pulvinata.*** (a) Functional classification of DEGs
537 identified for the *in planta Cf*, *in vitro Cf/Hp* and *in planta Cf/Hp* interactions. Red:
538 upregulated, stable: grey, blue: downregulated. The number of genes assigned to each
539 category is in parentheses. (b) Heatmap showing expression profiles of effector genes. The
540 red to blue gradient represents up- and downregulated expression, respectively. Genes with
541 an adjusted *P*-value ≥0.05 are indicated in gray as not detected (ND). Red arrowhead
542 indicates *Ecp2*. (c) Antimicrobial activity prediction for 56 effector genes upregulated during
543 the *in vitro Cf/Hp* interaction (determined using the AMAPEC program). Symbols denote
544 protein location predicted by EffectorP-fungi 3.0.
545
546

547 **Structural and functional similarity between *C. fulvum* Ecp2 effector and antifungal**
548 **killer toxin 4 proteins**

549 The Alphafold2-predicted structure of Ecp2 yielded high confidence scores, with a pLDDT
550 of 91.3 and a pTM of 0.872, indicating reliable local and global structures (Fig. **6a**). The
551 structural similarity search using the DALI server identified two killer toxin 4 (KP4)-like

proteins, ZtKP4 in *Zymoseptoria tritici* and UmVKP4 in *Ustilago maydis*, despite their low amino acid sequence similarity (2.9 and 36.9%, respectively) (Table **S8**). The comparative structural analysis showed that the overall arrangement of the α-helices and multiple β-sheet was conserved among these proteins (Fig. **6a** and **S7a**). The TM-score for Ecp2 relative to ZtKP4 was 0.81 and 0.59 relative to UmVKP4, supporting Ecp2 having the same structural fold as the KP4 protein family according to the SCOP and CATH classification criteria (Fig. **6b**).

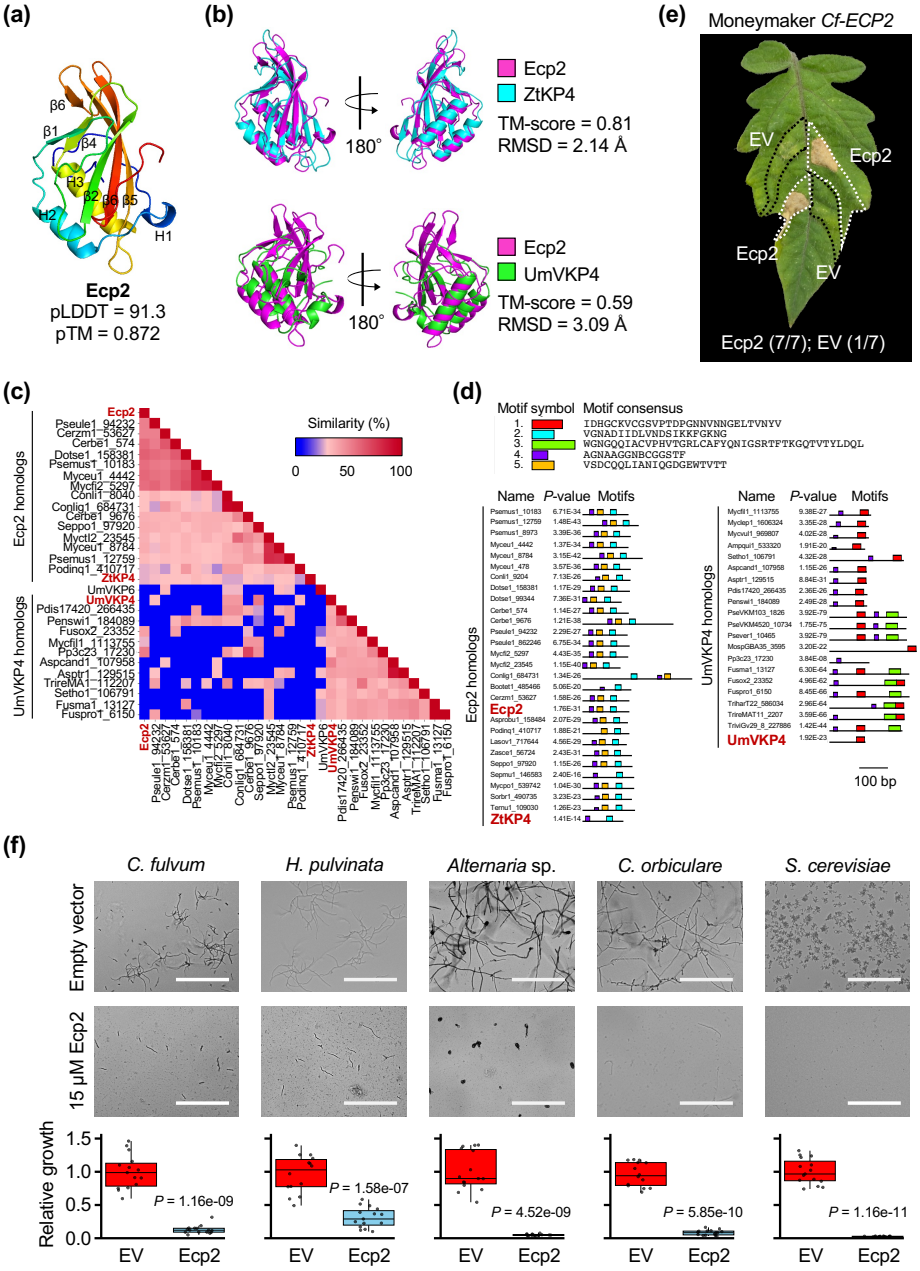

Fig. 6. Sequence dissimilarity and structural similarity between *Cladosporium fulvum* effector Ecp2 and killer toxin KP4 proteins. (a) Predicted 3D structure of Ecp2 generated using AlphaFold2. The color spectrum from blue to red indicates the N- to C-terminal

563 positions of residues. (b) Structural comparison of Ecp2 with ZtKP4 and UmVKP4 proteins.
564 The superposition of the aligned proteins was evaluated using TM-align, and the TM-score
565 and RMSD values are shown. (c) Heatmap showing sequence similarity among Ecp2, ZtKP4,
566 and UmVKP4 proteins as identified by BLASTp analysis. (d) Conserved motifs of proteins
567 identified by MEME motif analysis. (e) Representative tomato leaf from 4-week-old plant
568 carrying *Cf-ECP2* resistance gene at 6 days after infiltration with purified Ecp2 protein
569 produced by *Escherichia coli*. White dotted outline: area infiltrated with 1 μM Ecp2; black
570 dotted outline: infiltrated with control protein purified from *E. coli* harboring an empty vector
571 (EV). Numbers in parentheses indicate the number of leaves with a hypersensitive response
572 (HR) relative to the number of total leaves. (f) *In vitro* antifungal activity of Ecp2 against *C.*
573 *fulvum*, *H. pulvinata*, *Alternaria* sp., *Colletotrichum orbiculare*, and *Saccharomyces*
574 *cerevisiae*. Spores were cultured on 5% potato dextrose agar with or without Ecp2. Relative
575 hyphal length was determined 4 days after treatment. Bars = 250 μm. Significant differences
576 between EV and Ecp2 treatments were assessed using Student's *t*-test.
577
578
579 To explore the evolutionary relationships among these KP4-like proteins, we searched
580 for homologs of Ecp2, ZtKP4, and UmVKP4. Nineteen Ecp2 homologs were identified
581 across three fungal classes, while only one ZtKP4 homolog was detected in *Zymoseptoria*
582 *tritici* (syn. *Mycosphaerella graminicola*) (Table **S9**). A total of 188 UmVKP4 homologs
583 were found in 10 classes. Based on sequence similarity, these proteins clustered into two
584 groups; Ecp2 and ZtKP4 were placed in the same clade (Fig. **6c**). Motif analysis revealed
585 distinct conserved amino acid motifs in each group, and UmVKP4 group lacked an Hce2
586 domain (Fig. **6d**). While Ecp2 and ZtKP4 shared two conserved disulfide bonds, UmVKP4
587 had five, suggesting differences in structural stability and folding despite their shared overall
588 architecture (Fig. **S7b**). These results indicated that Ecp2 and UmVKP4 protein groups likely
589 originated from two distinct evolutionary lineages.
590 Given that Ecp2 is structurally and phylogenetically close to ZtKP4, which has
591 antifungal activity (de Guillen *et al*., 2024), we investigated the antifungal potential of Ecp2.
592 Infiltration of *Cf-ECP2* tomato leaves with recombinant Ecp2 (Fig. **S7c**) triggered a specific
593 HR (Fig. **6e**). At the high concentrations used, the active Ecp2 protein significantly inhibited
594 hyphal growth in diverse fungi: *C. fulvum*, *H. pulvinata*, *Alternaria* sp. isolated from tomato
595 fruits, the plant pathogen *Colletotrichum orbiculare* and the yeast *Saccharomyces cerevisiae*
596 (Fig. **6f**). Together, these results demonstrated that Ecp2 has a dual role: inducing *Cf-ECP2*-

597 mediated immunity in plant while inhibiting fungal growth. *H. pulvinata* exhibited
598 marginally higher resistance than the other tested fungi and yeast to Ecp2.
599
600 **Enrichment analysis of DEGs and KEGG pathways in tomato plants**
601 We also analyzed differential gene expression in tomato leaves inoculated with *C. fulvum*
602 or inoculated with *C. fulvum* followed by *H. pulvinata*, each compared with uninoculated
603 control leaves (Fig. **1a**). Infection by *C. fulvum* alone led to 3,231 upregulated and 4,980
604 downregulated genes, whereas in the presence of *H. pulvinata* (*in planta Cf/Hp*), 3,465 genes
605 were upregulated and 5,679 downregulated (Fig. **7a**). Among these, 1,619 up- and 2,153
606 downregulated genes were uniquely responsive to *H. pulvinata*, mapping to 35 and 33
607 enriched KEGG pathways, respectively (Fig. **7b**). Pathways associated with plant–pathogen
608 interaction, phytoalexin biosynthesis (stilbenoid, diarylheptanoid and gingerol), biosynthesis
609 of unsaturated fatty acids, other secondary metabolites, phenylpropanoid biosynthesis and
610 plant hormone signal transduction were induced when *H. pulvinata* parasitized *C. fulvum* in
611 leaves (Fig. **7b**). Genes encoding calcium-dependent protein kinases, PR1, RIN4, MAP
612 kinase, WRKY22 and defensins were highly expressed (Fig. **S8a**; Table **S10**). These results
613 indicated that *H. pulvinata* triggers plant immunity during its mycoparasitism of the pathogen
614 in tomato leaves. In contrast, pathways associated with photosynthesis antenna proteins and
615 porphyrin metabolism, which is involved in chlorophyll biosynthesis, were upregulated
616 during infection by *C. fulvum* alone, but significantly downregulated when parasitized by *H.*
617 *pulvinata* (Fig. **7b**; Fig. **S8b** and **c**), indicating that *H. pulvinata* triggered pronounced plant
618 resistance responses during mycoparasitism.
619 Strikingly, 13 amino acid biosynthesis and metabolism pathways were strongly activated
620 in the *in planta Cf/Hp* condition (Fig. **7b** and **c**). Although amino acid metabolism was
621 broadly repressed in both *C. fulvum* and *H. pulvinata* during mycoparasitism (Fig. **2b** and
622 **4b**), it was upregulated in tomato. The pronounced activation of amino acid biosynthesis
623 pathways in tomato suggests that the plant supplied amino acids to the mycoparasite *H.*
624 *pulvinata* during the tripartite interaction.

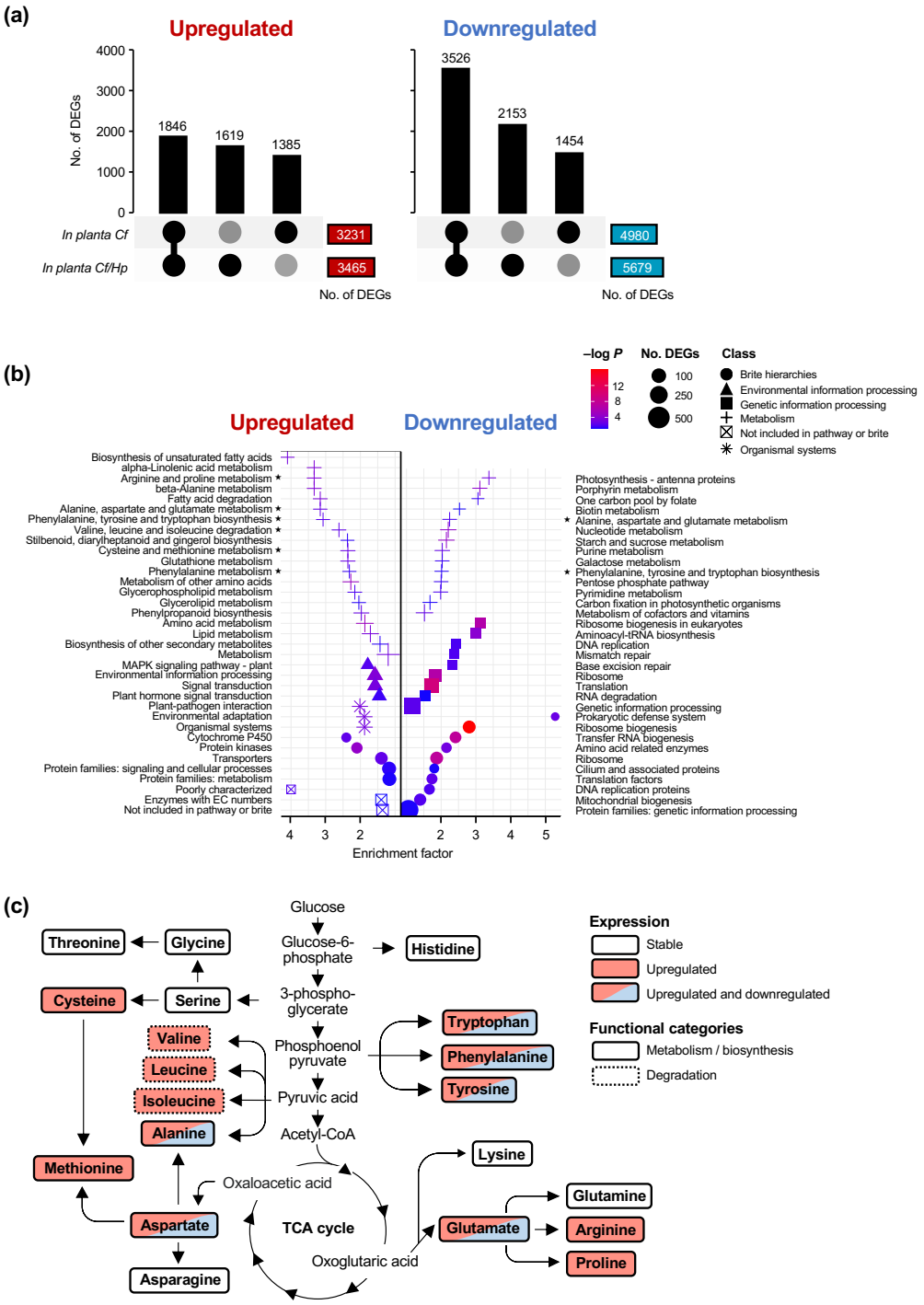

Fig. 7. Differentially expressed genes (DEGs) and enriched KEGG pathways in tomato plants. (a) UpSet plot of DEGs in the *in planta Cf* and *in planta Cf/Hp* conditions (see Fig. 1a). Healthy leaves were used as a control. Connected dots indicate shared DEGs; black single dots represent condition-specific DEGs. Vertical bars show the number of up- and downregulated genes; colored horizontal bars indicate the total number of DEGs detected in each interaction. (b) Bubble plot of KEGG pathway enrichment analysis based on the 1,619 and 2,153 DEGs shown in (a). Keys: color of symbols indicates significance level of

633 enrichment (–log adjusted *P*); size of symbol indicates the number of enriched DEGs in each
634 pathway; the symbol indicates the functional class of the enriched DEGs. Stars indicate
635 pathways highlighted in (c). (c) KEGG pathways involved in amino acid biosynthesis in
636 tomato.
637
638 **DISCUSSION**
639 In this study, we analyzed gene expression in tomato plants, the phytopathogenic fungus *C.*
640 *fulvum*, and mycoparasitic fungus *H. pulvinata* during the mycoparasitism of the pathogen
641 after it had infected its tomato host to capture their coordinated and distinct responses. We
642 thus discovered previously unrecognized aspects of molecular crosstalk and revealed how the
643 transcriptome of each organism was dynamically reprogrammed during the tripartite
644 interaction (Fig. **8**).
645

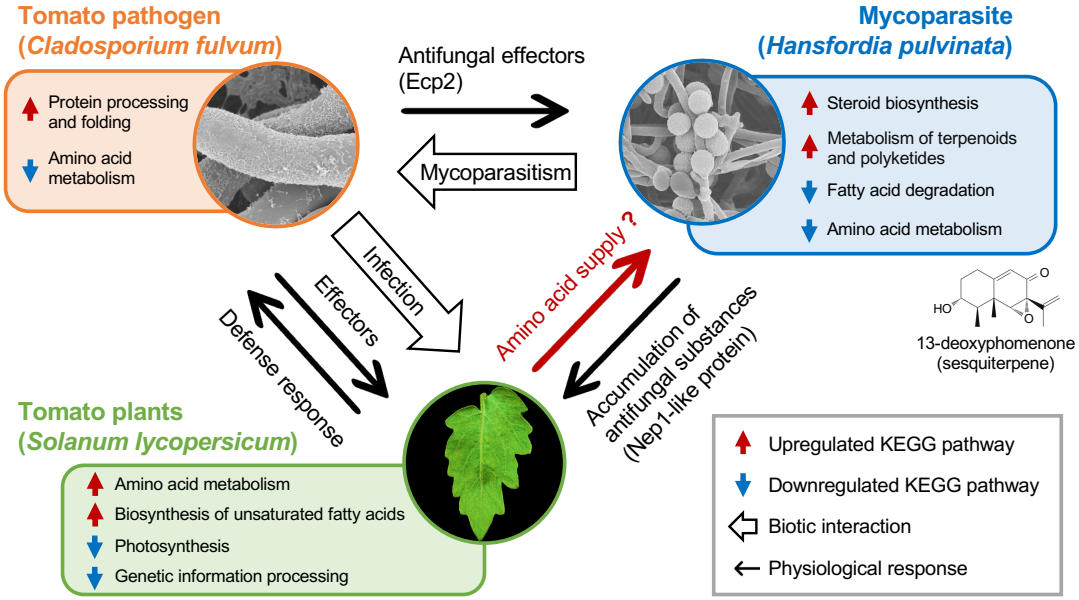

646
647 **Fig. 8. Overview of tripartite interaction among tomato plants, phytopathogen**
648 ***Cladosporium fulvum*, and mycoparasite *Hansfordia pulvinata*.** *C. fulvum* secretes effector
649 proteins that function as virulence factors in susceptible tomato cultivars and antifungal
650 proteins active against other fungi, but act as avirulence factors upon recognition by *Cf*-
651 resistant cultivars. *H. pulvinata* parasitizes *C. fulvum* and induces the production of apoplastic
652 antifungal substances in tomato plants via the Nep1-like protein HpNlp1. *H. pulvinata* also
653 activates the biosynthesis of the antifungal sesquiterpene 13-deoxyphomenone during
654 mycoparasitism. Other plant defense responses support this biocontrol effect. Pathways

655 related to amino acid biosynthesis in the three organisms suggest that nutrients from the plant
656 are supplied to *H. pulvinata*.
657
658
659 **Evolutionary and functional insights into an atypical NLP in the biocontrol**
660 **mycoparasite *H. pulvinata***
661 The identification of 165 secreted small proteins upregulated during mycoparasitism
662 highlights the central role of the secretome of *H. pulvinata*. Among them, HpNlp1, an
663 atypical NLP, lacked both necrosis-inducing activity or RLP23 receptor-mediated response in
664 plants, unlike canonical NLPs such as PsojNIP (Qutob *et al*., 2006; Böhm *et al*., 2014; Oome
665 *et al*., 2014). Instead, HpNlp1 accumulated antifungal substances in the apoplast and
666 inhibited spore germination of *C. fulvum*. Although *H. pulvinata* cannot grow independently
667 on tomato leaves (Iida *et al*., 2018), it entered tomato plants through stomata only in the
668 presence of *C. fulvum* (Fig. **S1b**), indicating that the two fungi overlap in the apoplastic
669 niche. Furthermore, the functional divergence of the NLPs between the pathogen and
670 mycoparasite indicates the evolutionary plasticity of NLP family. Despite its structural
671 similarity to PsojNIP, HpNlp1 has distinct biological functions, suggesting that subtle amino
672 acid modifications can drive functional divergence within the NLP family. If *H. pulvinata*
673 induced a strong necrotic or immune response in tomato, the host fungus *C. fulvum* would
674 decline, limiting its own nutrient supply. Therefore, the high upregulation of a noncytotoxic
675 NLP such as HpNlp1 during mycoparasitism is evolutionarily reasonable. Notably, the
676 *HpNLP1* gene was expressed in *H. pulvinata* when parasiting its host *in planta* and *in vitro*,
677 suggesting that it recognizes *C. fulvum* itself rather than plant-derived signals. Although
678 HpNlp1 did not directly inhibit *C. fulvum* growth, it indirectly promoted the accumulation of
679 antifungal metabolites, suggesting coevolution of *H. pulvinata* with not only its fungal host
680 *C. fulvum* but also tomato plants.
681 KEGG enrichment analysis indicated that *H. pulvinata* activated multiple secondary
682 metabolic pathways, particularly those related to terpenoids, polyketides, steroids and *DPH*
683 biosynthetic gene cluster, during mycoparasitism. These findings agree with previous
684 findings that *H. pulvinata* produces 13-deoxyformenone, an eremophilane-type
685 sesquiterpenoid, which is fungistatic to *C. fulvum* (Maeda *et al*., 2025). The production of
686 antifungal substances triggered by HpNlp1 in the tomato apoplast was correlated with the
687 induction of genes encoding defensins and phytoalexins, which were expressed only when *C.*
688 *fulvum* was parasitized by *H. pulvinata* in tomato leaves. Given that similar noncytotoxic

689 NLPs from the biocontrol oomycete *Pythium oligandrum* also induce plant defensins (Yang
690 *et al*., 2022), HpNlp1 may represent a conserved mechanism among biocontrol agents that
691 modulate plant immunity without causing cell death. *H. pulvinata* may employ a two-tiered
692 strategy to preserve the spores of its host fungus *C. fulvum*, combining a direct antifungal
693 sesquiterpenoid with an indirect, noncytotoxic protein, HpNlp1.
694
695 **Ecp2 effector as a novel antifungal protein in the pathogen *C. fulvum***
696 KP4 family proteins, broadly conserved in phytopathogenic fungi, are antifungal. For
697 instance, *U. maydis* UmVKP4 suppresses the growth of susceptible strains of the same
698 species by inhibiting calcium-dependent pathways that regulate the cell cycle and
699 morphogenesis (Gu *et al*., 1995; Gage *et al*., 2002). *Z. tritici* ZtKP4 has fungicidal activity
700 even against itself (de Guillen *et al*., 2024). Our structural modeling showed that *C. fulvum*
701 Ecp2 shared similarity with KP4 proteins and had broad-spectrum antifungal activity ranging
702 from filamentous fungi to yeast, including self-inhibition similar to that of ZtKP4. The β1-β2
703 loop in Ecp2 should functionally correspond to the β3–β4 loop of UmVKP4, which mediates
704 interactions with intracellular proteins (Gu *et al*., 1995). However, Ecp2 lacked the key lysine
705 residue (Lys42) that UmVKP4 requires for full antifungal activity (Gage *et al*., 2001),
706 suggesting a similar mechanism underlying antifungal action but involving an alternative
707 molecular interface. During the arms race between tomato and *C. fulvum*, a KP4-like
708 antifungal protein may have been diverted to Ecp2 effector. However, the structural basis
709 underlying *CfECP2*-mediated immune recognition and how Ecp2 acquired the dual ability to
710 interact with both fungal and plant targets remain unresolved.
711 Ecp2 was strongly expressed even during the *in vitro* mycoparasitism, suggesting a dual
712 role as both a virulence factor against plants and an antifungal protein in microbial
713 competition. A similar dual functionality is seen in the root endophyte *Serendipita* spp.,
714 where a chitinase encoding effector is induced during both plant colonization and microbial
715 interaction (Eichfeld *et al*., 2024). The vascular wilt fungus *Verticillium dahliae* secretes
716 antimicrobial effectors such as VdAve1 and VdAMP2 to gain an ecological advantage in the
717 soil biome (Snelders *et al*., 2020). The soil-borne pathogen *Rosellinia necatrix*, which causes
718 white root rot and is phylogenetically related to *V. dahliae*, secretes antimicrobial effector
719 proteins when it colonizes its host plant (Chavarro-Carrero *et al*., 2024). While the
720 rhizosphere harbors highly diverse and competitive microbial communities, the diversity of
721 the microbial community in the endosphere such as the apoplastic space is generally
722 relatively low (Snelders *et al*., 2022) because colonization of the apoplast is typically

723 restricted to specialized microbes that can secrete effectors to suppress host immunity
724 (Rocafort *et al*., 2020). Consequently, the potential role of antimicrobial effectors where
725 competition is relatively low is still unclear. In fact, despite previous predictions that some
726 apoplastic effectors produced by *C. fulvum* may have antimicrobial activity, no direct
727 evidence had been found (Mesarich *et al*., 2018). Our finding indicates the potential for *C.*
728 *fulvum* not only to utilize effectors for efficient colonization but also to mediate microbial
729 competition in the endosphere and phyllosphere. Although *H. pulvinata* was moderately
730 tolerant of Ecp2, the molecular basis for this tolerance during mycoparasitism remains
731 unclear.
732 The Hce2 (Homologs of *C. fulvum* Ecp2) superfamily is widely conserved across the
733 *Ascomycota* and *Basidiomycota*, suggesting that its origin predates the divergence of the
734 *Dikarya* lineage (Stergiopoulos *et al*., 2012). In contrast, *U. maydis* UmVKP4, which shares
735 structural similarity with Ecp2, lacks the Hce2 domain and shared sequence motifs, and
736 differs in the number of disulfide bonds (Fig. **S7b**). These findings suggest that UmVKP4
737 represents a case of convergent evolution, resulting in structural resemblance to Ecp2 and
738 ZtKP4. Molecular evolutionary analyses suggest that the amino acid substitution underlying
739 Hce2 function diversification was fixed early in evolution (Stergiopoulos *et al*., 2012).
740 Ancestral Hce2 proteins may initially act as antimicrobial factors to provide competitive
741 advantages in microbe-rich habitats and have been co-opted as an effector to inhibit plant
742 immunity. Mutations in effector genes that allow *C. fulvum* to evade *Cf* resistance in plants
743 may increase its susceptibility to antagonistic microbes such as *H. pulvinata*. This hypothesis
744 suggests that mycoparasitic biocontrol agents can circumvent the classical arms race between
745 plant and pathogen, providing a sustainable disease management.
746
747 **Potential metabolic trade-offs in amino acid pathways between fungi and tomato plants**
748 The physiological changes found in tomato plants highlight the dynamic interplay between
749 microbial interference and plant defense responses. The expression of genes in multiple
750 amino acid biosynthetic pathways were enhanced only when *H. pulvinata* parasitized *C.*
751 *fulvum* in tomato leaves. Amino acids are key mediators of plant–microbe interactions,
752 functioning as signaling molecules that activate defense and as nutritional sources that
753 pathogens exploit (Moormann *et al*., 2022; Tünnermann *et al*., 2022). Indeed, infection by *C.*
754 *fulvum* leads to the accumulation of free amino acids in the apoplast (Solomon & Oliver,
755 2001). Because the acquisition of plant-derived amino acids is energetically advantageous to
756 microbes, many plant pathogens modulate expression of genes encoding amino acid

757 transporters to optimize uptake (Sonawala *et al*., 2018). Thus, the regulation of amino acid
758 assimilation and transport in plants can be a decisive factor shaping the outcome of plant–
759 pathogen interactions.
760 In contrast, amino acid biosynthetic pathways in *H. pulvinata* and *C. fulvum* were
761 downregulated during the mycoparasitism on the membrane and the plant, suggesting that
762 tomato-derived amino acids could be shared or sequentially utilized by these fungi (Fig. **8**).
763 Although amino acids are fundamental primary metabolites during fungal vegetative growth,
764 the metabolic profile of *H. pulvinata*, which had vigorous hyphal growth during
765 mycoparasitism, deviated from this conventional paradigm. Although *C. fulvum* may also
766 acquire amino acids from plants, these resources are likely reallocated to *H. pulvinata*, the
767 ultimate beneficiary. In this metabolic trade-off, tomato plants invest in amino acids that
768 benefit *H. pulvinata*, while receiving biocontrol protection in return (Fig. **8**). Similar
769 strategies have been reported for the biocontrol fungus *Pseudozyma flocculosa*, which
770 transiently suppresses photosynthesis to promote amino acid release (Laur *et al*., 2018). The
771 mycoparasitic fungus *Trichoderma erinaceum* exploits environmental amino acids to enhance
772 the synthesis of antifungal secondary metabolites derived from amino acids (Guo *et al*.,
773 2020). Together, these results suggested that shifts in amino acid metabolism enable *H.*
774 *pulvinata* to harness pathogen-induced plant responses for its benefit.
775
776 **Mycoparasitism by *H. pulvinata* modulates plant immunity and pathogen growth**
777 In conclusion, the mycoparasite *H. pulvinata* actively reprogrammed gene expression and
778 physiological responses in the pathogen *C. fulvum* and its tomato host to establish a stable
779 tripartite interaction (Fig. **8**). *H. pulvinata* induced expression of the 13-deoxyphomenone
780 biosynthetic gene cluster in tomato, thereby directly suppressing *C. fulvum*. It also enhanced
781 plant resistance, leading to the accumulation of antimicrobial substances in the apoplast and
782 thus indirectly further suppressing *C. fulvum*. In turn, *C. fulvum* secreted effectors such as
783 Ecp2, which functioned to induce both fungal competition and plant immunity. *H. pulvinata*
784 is likely to tolerate or overcome these antifungal effectors, but the underlying mechanisms
785 remain unclear. The tomato plant reprogrammed amino acid metabolism and defense
786 response pathways, orchestrating distinct strategies against beneficial and pathogenic
787 microbes. Collectively, these findings underscore the dynamic interplay of plant–pathogen–
788 mycoparasite interactions, demonstrating that *H. pulvinata* simultaneously strengthens tomato
789 immunity and represses *C. fulvum* virulence via direct antagonism and modulation of plant
790 metabolic pathways.

ACKNOWLEDGEMENTS

This work was supported by a Grant-in-Aid for Scientific Research from JSPS (20H02993 and 24K08919) and the Research and Implementation Promotion Program through Open Innovation Grants (JPJ011937) from the Project of the Bio-oriented Technology Research Advancement Institution (BRAIN) (Y. Iida). We are grateful to K. Ikeda for providing fungal strains, M.H.A.J. Joosten for *Cf-ECP2* tomato seeds, D. Takemoto for the *psojNIP* gene, F. Takken for pSfinx, and Y. Kubo for the *C. orbiculare* strain. We thank Y. Kubo, M.Z. Fanani and S. Kodama for valuable suggestions, C. Tanaka for laboratory management.

COMPETING INTERESTS

The authors declare that they have no commercial or financial relationships that could be construed as a potential conflict of interest.

AUTHOR CONTRIBUTIONS

YI designed the study and managed the research funds. KM, HS and TaS performed RNA-seq and analyzed the data. KM, MK, MO, and TK analyzed NLPs. ToS conducted electron microscopy and EI developed a microscopic observation protocol. KM and KS studied the Ecp2 protein. KM and YI wrote the manuscript. All authors reviewed and approved the final version.

DATA AVAILABILITY

Genomic sequences for *C. fulvum* strain Race5_Kim and *H. pulvinata* strain 414-3 are available as accessions PRJNA565804 and PRJDB8178 at NCBI BioProject, respectively (Sushida *et al*., 2019; Zaccaron & Stergiopoulos, 2024). Tomato genome data were obtained from the Solanaceae Genomics Network (Hosmani *et al*., 2019). Additional genomes are accessible via JGI MycoCosm (mycocosm.jgi.doe.gov) and the DDBJ/EMBL/GenBank repository (www.ncbi.nlm.nih.gov). Custom scripts and supporting datasets were deposited at Figshare (doi.org/10.6084/m9.figshare.30265009).

REFERENCES

Bailey TL, Johnson J, Grant CE, Noble WS. 2015. The MEME Suite. *Nucleic Acids Research*. 2015 Jul 1;43(W1):W39-49. doi: 10.1093/nar/gkv416. Epub 2015 May 7. PMID: 25953851; PMCID: PMC4489269.

825 **Berg S, Kutra D, Kroeger T, Straehle CN, Kausler BX, Haubold C, Schiegg M, Ales J,**
826 **Beier T, Rudy M,** et al. 2019. ilastik: interactive machine learning for (bio)image
827 analysis. *Nature Methods*. 2019 Dec;16(12):1226-1232. doi: 10.1038/s41592-019-0582-
828 9. Epub 2019 Sep 30. PMID: 31570887.
829 **Blin K, Shaw S, Augustijn HE, Reitz ZL, Biermann F, Alanjary M, Fetter A, Terlouw**
830 **BR, Metcalf WW, Helfrich EJN,** et al. 2023. antiSMASH 7.0: new and improved
831 predictions for detection, regulation, chemical structures and visualisation. *Nucleic Acids*
832 *Research*. 2023 Jul 5;51(W1):W46-W50. doi: 10.1093/nar/gkad344. PMID: 37140036;
833 PMCID: PMC10320115.
834 **Böhm H, Albert I, Oome S, Raaymakers TM, Van den Ackerveken G, Nürnberger T.**
835 2014. A conserved peptide pattern from a widespread microbial virulence factor triggers
836 pattern-induced immunity in *Arabidopsis*. *PLOS Pathogens*. 2014 Nov
837 6;10(11):e1004491. doi: 10.1371/journal.ppat.1004491. PMID: 25375108; PMCID:
838 PMC4223075.
839 **Bolger AM, Lohse M, Usadel B**. 2014. Trimmomatic: a flexible trimmer for Illumina
840 sequence data. *Bioinformatics*. 2014 Aug 1;30(15):2114-20. doi:
841 10.1093/bioinformatics/btu170. Epub 2014 Apr 1. PMID: 24695404; PMCID:
842 PMC4103590.
843 **Capella-Gutiérrez S, Silla-Martínez JM, Gabaldón T.** 2009. trimAl: a tool for automated
844 alignment trimming in large-scale phylogenetic analyses. *Bioinformatics*. Aug
845 1;25(15):1972-3. doi: 10.1093/bioinformatics/btp348. Epub 2009 Jun 8. PMID:
846 19505945; PMCID: PMC2712344.
847 **Chaillot J, Tebbji F, Remmal A, Boone C, Brown GW, Bellaoui M, Sellam A.** 2015. The
848 Monoterpene Carvacrol Generates Endoplasmic Reticulum Stress in the Pathogenic
849 Fungus *Candida albicans*. *Antimicrobial Agents and Chemotherapy*. 2015
850 Aug;59(8):4584-92. doi: 10.1128/AAC.00551-15. Epub 2015 May 26. PMID: 26014932;
851 PMCID: PMC4505245.
852 **Chavarro-Carrero EA, Snelders NC, Torres DE, Kraege A, López-Moral A, Petti GC,**
853 **Punt W, Wieneke J, García-Velasco R, López-Herrera CJ,** et al. 2024. The soil-borne
854 white root rot pathogen *Rosellinia necatrix* expresses antimicrobial proteins during host
855 colonization. *PLOS Pathogens*. 2024 Jan 18;20(1):e1011866. doi:
856 10.1371/journal.ppat.1011866. PMID: 38236788; PMCID: PMC10796067.
857 **Chen C, Wu Y, Li J, Wang X, Zeng Z, Xu J, Liu Y, Feng J, Chen H, He Y,** et al. 2023.
858 TBtools-II: A "one for all, all for one" bioinformatics platform for biological big-data

859 mining. *Molecular Plant*. 2023 Nov 6;16(11):1733-1742. doi:
860 10.1016/j.molp.2023.09.010. Epub 2023 Sep 22. PMID: 37740491.
861 **de Guillen K, Mammri L, Gracy J, Padilla A, Barthe P, Hoh F, Lahfa M, Rouffet J,**
862 **Petit-Houdenot Y, Kroj T,** et al. 2024. *Zymoseptoria tritici* effectors structurally related
863 to killer proteins UmV-KP4 and UmV-KP6 are toxic to fungi, and define extended
864 protein families in fungi. *bioRxiv*. 2024 Oct 14:2024.10.14.618152.
865 doi:10.1101/2024.10.14.618152.
866 **de la Rosa S, Schol CR, Ramos Peregrina Á, Winter DJ, Hilgers AM, Maeda K, Iida Y,**
867 **Tarallo M, Jia R, Beenen HG,** et al. 2024. Sequential breakdown of the *Cf-9* leaf mold
868 resistance locus in tomato by *Fulvia fulva*. *New Phytologist*. 2024 Aug;243(4):1522-
869 1538. doi: 10.1111/nph.19925. Epub 2024 Jun 24. PMID: 38922927.
870 **de Jonge R, van Esse HP, Kombrink A, Shinya T, Desaki Y, Bours R, van der Krol S,**
871 **Shibuya N, Joosten MH, Thomma BP.** 2010. Conserved fungal LysM effector Ecp6
872 prevents chitin-triggered immunity in plants. *Science*. 2010 Aug 20;329(5994):953-5.
873 doi: 10.1126/science.1190859. PMID: 20724636.
874 **de Wit PJGM, van der Burgt A, Ökmen B, Stergiopoulos I, Abd-Elsalam KA, Aerts AL,**
875 **Bahkali AH, Beenen HG, Chettri P, Cox MP**, et al. 2012. The genomes of the fungal
876 plant pathogens *Cladosporium fulvum* and *Dothistroma septosporum* reveal adaptation to
877 different hosts and lifestyles but also signatures of common ancestry. *PLOS Genetics*.
878 2012;8(11):e1003088. doi: 10.1371/journal.pgen.1003088. Epub 2012 Nov 29. Erratum
879 in: PLoS Genet. 2015 Dec 22;11(12):e1005775. doi: 10.1371/journal.pgen.1005775.
880 PMID: 23209441; PMCID: PMC3510045.
881 **de Wit PJGM, Joosten MHAJ, Thomma BHPJ, Stergiopoulos I.** 2009. Gene for gene
882 models and beyond: the *Cladosporium fulvum*–tomato pathosystem. *Plant relationships*.
883 Berlin, Heidelberg: Springer; 2009. p. 135–156. (The Mycota; vol 5). doi:10.1007/978-3-
884 540-87407-2_7.
885 **Eichfeld R, Mahdi LK, de Quattro C, Armbruster L, Endeshaw AB, Miyauchi S,**
886 **Hellmann MJ, Cord-Landwehr S, Peterson D, Singan V,** et al. 2024. Transcriptomics
887 reveal a mechanism of niche defense: two beneficial root endophytes deploy an
888 antimicrobial GH18-CBM5 chitinase to protect their hosts. *New Phytologist*. 2024
889 Nov;244(3):980-996. doi: 10.1111/nph.20080. Epub 2024 Sep 3. PMID: 39224928.
890 **Emms DM, Kelly S.** 2019. OrthoFinder: phylogenetic orthology inference for comparative
891 genomics. *Genome Biology*. 2019 Nov 14;20(1):238. doi: 10.1186/s13059-019-1832-y.
892 PMID: 31727128; PMCID: PMC6857279.

Gage MJ, Bruenn J, Fischer M, Sanders D, Smith TJ. 2001. KP4 fungal toxin inhibits growth in *Ustilago maydis* by blocking calcium uptake. *Molecular Microbiology*. 2001 Aug;41(4):775-85. doi: 10.1046/j.1365-2958.2001.02554.x. PMID: 11532143.

Gage MJ, Rane SG, Hockerman GH, Smith TJ. 2002. The virally encoded fungal toxin KP4 specifically blocks L-type voltage-gated calcium channels. *Molecular Pharmacology*. 2002 Apr;61(4):936-44. doi: 10.1124/mol.61.4.936. PMID: 11901234.

Gene Ontology Consortium; Aleksander SA, Balhoff J, Carbon S, Cherry JM, Drabkin HJ, Ebert D, Feuermann M, Gaudet P, Harris NL, et al. 2023. The Gene Ontology knowledgebase in 2023. *Genetics*. 2023 May 4;224(1):iyad031. doi: 10.1093/genetics/iyad031. PMID: 36866529; PMCID: PMC10158837.

Gíslason MH, Nielsen H, Almagro Armenteros JJ, Johansen AR. 2021. Prediction of GPI-anchored proteins with pointer neural networks. *Current Research in Biotechnology*. 2021;3:6-13. doi:10.1016/j.crbiot.2021.01.001.

Griffiths S, Mesarich CH, Overdijk EJR, Saccomanno B, de Wit PJGM, Collemare J. 2018. Down-regulation of cladofulvin biosynthesis is required for biotrophic growth of *Cladosporium fulvum* on tomato. *Molecular Plant Pathology*. 2018 Feb;19(2):369-380. doi: 10.1111/mpp.12527. Epub 2017 Feb 6. PMID: 27997759; PMCID: PMC6638085.

Gu F, Khimani A, Rane SG, Flurkey WH, Bozarth RF, Smith TJ. 1995. Structure and function of a virally encoded fungal toxin from *Ustilago maydis*: a fungal and mammalian Ca2+ channel inhibitor. *Structure*. 1995 Aug 15;3(8):805-14. doi: 10.1016/s0969-2126(01)00215-5. PMID: 7582897.

Guo YW, Gong BQ, Yuan J, Li HJ, Mahmud T, Huang Y, Li JF, Yang DP, Lan WJ. 2020. l-Phenylalanine Alters the Privileged Secondary Metabolite Production in the Marine-Derived Fungus T*richoderma erinaceum* F1-1. *Journal of Natural Products*. 2020 Jan 24;83(1):79-87. doi: 10.1021/acs.jnatprod.9b00710. Epub 2019 Dec 30. PMID: 31886665.

Holm L. 2022. Dali server: structural unification of protein families. *Nucleic Acids Research*. 2022 Jul 5;50(W1):W210-W215. doi: 10.1093/nar/gkac387. PMID: 35610055; PMCID: PMC9252788.

Hosmani PS, Flores-Gonzalez M, van de Geest H, Maumus F, Bakker LV, Schijlen E, van Haarst J, Cordewener J, Sanchez-Perez G, Peters S, et al. 2019. An improved de novo assembly and annotation of the tomato reference genome using single-molecule sequencing, Hi-C proximity ligation and optical maps. *bioRxiv*. 2019;767764. doi:10.1101/767764

927 **Iida Y, Ikeda K, Sakai H, Nakagawa H, Nishi O, Higashi Y.** 2018. Evaluation of the
928 potential biocontrol activity of *Dicyma pulvinata* against *Cladosporium fulvum*, the
929 causal agent of tomato leaf mold. *Plant Pathology*. 2018;67(9):1883–1890.
930 doi:10.1111/ppa.12916.
931 **Iida Y, van 't Hof P, Beenen H, Mesarich C, Kubota M, Stergiopoulos I, Mehrabi R,**
932 **Notsu A, Fujiwara K, Bahkali A,** et al. 2015. Novel Mutations Detected in Avirulence
933 Genes Overcoming Tomato *Cf* Resistance Genes in Isolates of a Japanese Population of
934 *Cladosporium fulvum*. *PLoS One*. 2015 Apr 22;10(4):e0123271. doi:
935 10.1371/journal.pone.0123271. PMID: 25902074; PMCID: PMC4406682.
936 **Joosten MH.** 2012. Isolation of apoplastic fluid from leaf tissue by the vacuum infiltration-
937 centrifugation technique. *Methods in Molecular Biology*. 2012;835:603-10. doi:
938 10.1007/978-1-61779-501-5_38. PMID: 22183681.
939 **Kanehisa M, Furumichi M, Sato Y, Matsuura Y, Ishiguro-Watanabe M.** 2025. KEGG:
940 biological systems database as a model of the real world. *Nucleic Acids Research*. 2025
941 Jan 6;53(D1):D672-D677. doi: 10.1093/nar/gkae909. PMID: 39417505; PMCID:
942 PMC11701520.
943 **Katoh K., Standley DM.** 2013. MAFFT multiple sequence alignment software version 7:
944 improvements in performance and usability. *Molecular biology and*
945 *evolution*. Apr;30(4):772-80. doi: 10.1093/molbev/mst010. Epub 2013 Jan 16. PMID:
946 23329690; PMCID: PMC3603318.
947 **Kim D, Paggi JM, Park C, Bennett C, Salzberg SL.** 2019. Graph-based genome alignment
948 and genotyping with HISAT2 and HISAT-genotype. *Nature Biotechnology*. 2019
949 Aug;37(8):907-915. doi: 10.1038/s41587-019-0201-4. Epub 2019 Aug 2. PMID:
950 31375807; PMCID: PMC7605509.
951 **Kourelis J, Malik S, Mattinson O, Krauter S, Kahlon PS, Paulus JK, van der Hoorn**
952 **RAL.** 2020. Evolution of a guarded decoy protease and its receptor in solanaceous
953 plants. *Nature Communications*. 2020 Sep 2;11(1):4393. doi: 10.1038/s41467-020-
954 18069-5. Erratum in: *Nature Communications*. 2024 Mar 13;15(1):2278. doi:
955 10.1038/s41467-024-46611-2. PMID: 32879321; PMCID: PMC7468133.
956 **Laur J, Ramakrishnan GB, Labbé C, Lefebvre F, Spanu PD, Bélanger RR.** 2018.
957 Effectors involved in fungal-fungal interaction lead to a rare phenomenon of
958 hyperbiotrophy in the tritrophic system biocontrol agent-powdery mildew-plant. *New*
959 *Phytologist*. 2018 Jan;217(2):713-725. doi: 10.1111/nph.14851. Epub 2017 Oct 18.
960 PMID: 29044534; PMCID: PMC6079639.

Li H, Handsaker B, Wysoker A, Fennell T, Ruan J, Homer N, Marth G, Abecasis G, Durbin R; 1000 Genome Project Data Processing Subgroup. 2009. The Sequence Alignment/Map format and SAMtools. *Bioinformatics*. 2009 Aug 15;25(16):2078-9. doi: 10.1093/bioinformatics/btp352. Epub 2009 Jun 8. PMID: 19505943; PMCID: PMC2723002.

Love MI, Huber W, Anders S. 2014. Moderated estimation of fold change and dispersion for RNA-seq data with DESeq2. *Genome Biology*. 2014;15(12):550. doi: 10.1186/s13059-014-0550-8. PMID: 25516281; PMCID: PMC4302049.

Luderer R, Takken FL, de Wit PJGM, Joosten MH. 2002. *Cladosporium fulvum* overcomes *Cf-2*-mediated resistance by producing truncated AVR2 elicitor proteins. Molecular *Microbiology*. 2002 Aug;45(3):875-84. doi: 10.1046/j.1365-2958.2002.03060.x. PMID: 12139631.

Ma L, Lukasik E, Gawehns F, Takken FL. 2012. The use of agroinfiltration for transient expression of plant resistance and fungal effector proteins in *Nicotiana benthamiana* leaves. *Methods in Molecular Biology*. 2012;835:61-74. doi: 10.1007/978-1-61779-501-5_4. PMID: 22183647.

Madeira F, Madhusoodanan N, Lee J, Eusebi A, Niewielska A, Tivey ARN, Lopez R, Butcher S. 2024. The EMBL-EBI Job Dispatcher sequence analysis tools framework in 2024. *Nucleic Acids Research*. 2024 Jul 5;52(W1):W521-W525. doi: 10.1093/nar/gkae241. PMID: 38597606; PMCID: PMC11223882.

Maeda K, Sumita T, Nishi O, Sushida H, Higashi Y, Nakagawa H, Suzuki T, Iwao E, Fanani MZ, Nishiya Y, Iida Y. 2025. Adaptive evolution of sesquiterpene deoxyphomenone in mycoparasitism by *Hansfordia pulvinata* associated with horizontal gene transfer from *Aspergillus* species. *mBio*. 2025 Apr 9;16(4):e0400724. doi: 10.1128/mbio.04007-24. Epub 2025 Mar 20. PMID: 40111082; PMCID: PMC11980549.

Mesarich CH, Griffiths SA, van der Burgt A, Okmen B, Beenen HG, Etalo DW, Joosten MH, de Wit PJGM. 2014. Transcriptome sequencing uncovers the *Avr5* avirulence gene of the tomato leaf mold pathogen *Cladosporium fulvum*. *Molecular Plant-Microbe Interactions*. 2014 Aug;27(8):846-57. doi: 10.1094/MPMI-02-14-0050-R. PMID: 24678832.

Mesarich CH, Ökmen B, Rovenich H, Griffiths SA, Wang C, Karimi Jashni M, Mihajlovski A, Collemare J, Hunziker L, Deng CH, et al. 2018. Specific Hypersensitive Response-Associated Recognition of New Apoplastic Effectors from *Cladosporium fulvum* in Wild Tomato. *Molecular Plant-Microbe Interactions*. 2018

995 Jan;31(1):145-162. doi: 10.1094/MPMI-05-17-0114-FI. Epub 2017 Nov 16. PMID:
996 29144204.
997 **Mesarich CH, Barnes I, Bradley EL, de la Rosa S, de Wit PJGM, Guo Y, Griffiths SA,**
998 **Hamelin RC, Joosten MHAJ, Lu M,** et al. 2023. Beyond the genomes of *Fulvia fulva*
999 (syn. *Cladosporium fulvum*) and *Dothistroma septosporum*: New insights into how these
1000 fungal pathogens interact with their host plants. *Molecular Plant Pathology*. 2023
1001 May;24(5):474-494. doi: 10.1111/mpp.13309. Epub 2023 Feb 15. PMID: 36790136;
1002 PMCID: PMC10098069.
1003 **Mesny F, Wolf V, López-Moral A, Kraege A, Punt W, Park J, Zhu J, Sato Y, Thomma**
1004 **BPHJ.** 2024. Plant-associated fungi co-opt ancient antimicrobials for host manipulation.
1005 *bioRxiv*. Preprint posted online 2024 Jan 4. doi:10.1101/2024.01.04.574150.
1006 **Mirdita M, Schütze K, Moriwaki Y, Heo L, Ovchinnikov S, Steinegger M**. 2022.
1007 ColabFold: making protein folding accessible to all. *Nature Methods*. 2022
1008 Jun;19(6):679-682. doi: 10.1038/s41592-022-01488-1. Epub 2022 May 30. PMID:
1009 35637307; PMCID: PMC9184281.
1010 **Mistry J, Chuguransky S, Williams L, Qureshi M, Salazar GA, Sonnhammer ELL,**
1011 **Tosatto SCE, Paladin L, Raj S, Richardson LJ**, et al. 2021. Pfam: The protein families
1012 database in 2021. *Nucleic Acids Research*. 2021 Jan 8;49(D1):D412-D419. doi:
1013 10.1093/nar/gkaa913. PMID: 33125078; PMCID: PMC7779014.
1014 **Moormann J, Heinemann B, Hildebrandt TM.** 2022. News about amino acid metabolism
1015 in plant-microbe interactions. *Trends in Biochemical Sciences*. 2022 Oct;47(10):839-850.
1016 doi: 10.1016/j.tibs.2022.07.001. Epub 2022 Aug 1. PMID: 35927139.
1017 **Oome S, Raaymakers TM, Cabral A, Samwel S, Böhm H, Albert I, Nürnberger T, Van**
1018 **den Ackerveken G.** 2014. Nep1-like proteins from three kingdoms of life act as a
1019 microbe-associated molecular pattern in *Arabidopsis*. *Proceedings of the National*
1020 *Academy of Sciences, USA*. 2014 Nov 25;111(47):16955-60. doi:
1021 10.1073/pnas.1410031111. Epub 2014 Nov 3. PMID: 25368167; PMCID: PMC4250136.
1022 **Peresse M, Le Picard D.** 1980. *Hansfordia pulvinata*, mycoparasite destructeur du
1023 *Cladosporium fulvum*. *Mycopathologia* 1980. 71:23–30.
1024 **Qutob D, Kamoun S, Gijzen M.** 2002. Expression of a *Phytophthora sojae* necrosis-
1025 inducing protein occurs during transition from biotrophy to necrotrophy. *The Plant*
1026 *Journal*. 2002 Nov;32(3):361-73. doi: 10.1046/j.1365-313x.2002.01439.x. PMID:
1027 12410814.

1028 **Qutob D, Kemmerling B, Brunner F, Küfner I, Engelhardt S, Gust AA, Luberacki B,**
1029 **Seitz HU, Stahl D, Rauhut T,** et al. 2006. Phytotoxicity and innate immune responses
1030 induced by Nep1-like proteins. *The Plant Cell*. 2006 Dec;18(12):3721-44. doi:
1031 10.1105/tpc.106.044180. Epub 2006 Dec 28. PMID: 17194768; PMCID: PMC1785393.
1032 **R Core Team R.** 2024. *R: a language and environment for statistical computing*. Vienna,
1033 Austria: R Foundation for Statistical Computing.
1034 **Rocafort M, Fudal I, Mesarich CH.** 2020. Apoplastic effector proteins of plant-associated
1035 fungi and oomycetes. *Current Opinion in Plant Biology*. 2020 Aug;56:9-19. doi:
1036 10.1016/j.pbi.2020.02.004. Epub 2020 Apr 2. PMID: 32247857.
1037 **Rooney HC, Van't Klooster JW, van der Hoorn RA, Joosten MH, Jones JD, de Wit**
1038 **PJGM.** 2005. Cladosporium Avr2 inhibits tomato Rcr3 protease required for *Cf-2*-
1039 dependent disease resistance. *Science*. 2005 Jun 17;308(5729):1783-6. doi:
1040 10.1126/science.1111404. Epub 2005 Apr 21. Erratum in: Science. 2005 Oct
1041 7;310(5745):54. PMID: 15845874.
1042 **Seidl MF, Van den Ackerveken G.** 2019. Activity and Phylogenetics of the Broadly
1043 Occurring Family of Microbial Nep1-Like Proteins. *Annual Review of Phytopathology*.
1044 2019 Aug 25;57:367-386. doi: 10.1146/annurev-phyto-082718-100054. Epub 2019 Jul 5.
1045 PMID: 31283435.
1046 **Shabab M, Shindo T, Gu C, Kaschani F, Pansuriya T, Chintha R, Harzen A, Colby T,**
1047 **Kamoun S, van der Hoorn RA.** 2008. Fungal effector protein AVR2 targets
1048 diversifying defense-related cys proteases of tomato. *The Plant Cell*. 2008
1049 Apr;20(4):1169-83. doi: 10.1105/tpc.107.056325. Epub 2008 Apr 30. PMID: 18451324;
1050 PMCID: PMC2390736.
1051 **Shimodaira H.** 2002. An approximately unbiased test of phylogenetic tree selection. Syst
1052 Biol. Jun;51(3):492-508. doi: 10.1080/10635150290069913. PMID: 12079646.
1053 **Snelders NC, Rovenich H, Petti GC, Rocafort M, van den Berg GCM, Vorholt JA,**
1054 **Mesters JR, Seidl MF, Nijland R, Thomma BPHJ.** 2020. Microbiome manipulation
1055 by a soil-borne fungal plant pathogen using effector proteins. *Nature Plants*. 2020
1056 Nov;6(11):1365-1374. doi: 10.1038/s41477-020-00799-5. Epub 2020 Nov 2. PMID:
1057 33139860.
1058 **Snelders NC, Rovenich H, Thomma BPHJ.** 2022. Microbiota manipulation through the
1059 secretion of effector proteins is fundamental to the wealth of lifestyles in the fungal
1060 kingdom. *FEMS Microbiology Reviews*. 2022 Sep 2;46(5):fuac022. doi:
1061 10.1093/femsre/fuac022. PMID: 35604874; PMCID: PMC9438471.

1062 **Stamatakis A.** 2014. RAxML version 8: a tool for phylogenetic analysis and post-analysis of
1063 large phylogenies. *Bioinformatics*. May 1;30(9):1312-3. doi:
1064 10.1093/bioinformatics/btu033. Epub 2014 Jan 21. PMID: 24451623; PMCID:
1065 PMC3998144.
1066 **Solomon PS, Oliver RP.** 2001. The nitrogen content of the tomato leaf apoplast increases
1067 during infection by *Cladosporium fulvum*. *Planta*. 2001 Jun;213(2):241-9. doi:
1068 10.1007/s004250000500. PMID: 11469589.
1069 **Sonawala U, Dinkeloo K, Danna CH, McDowell JM, Pilot G.** 2018. Review: Functional
1070 linkages between amino acid transporters and plant responses to pathogens. *Plant*
1071 *Science*. 2018 Dec;277:79-88. doi: 10.1016/j.plantsci.2018.09.009. Epub 2018 Sep 19.
1072 PMID: 30466603.
1073 **Sperschneider J, Dodds PN.** 2022. EffectorP 3.0: Prediction of Apoplastic and Cytoplasmic
1074 Effectors in Fungi and Oomycetes. *Molecular Plant-Microbe Interactions*. 2022
1075 Feb;35(2):146-156. doi: 10.1094/MPMI-08-21-0201-R. Epub 2022 Feb 1. PMID:
1076 34698534.
1077 **Sperschneider J, Catanzariti AM, DeBoer K, Petre B, Gardiner DM, Singh KB, Dodds**
1078 **PN, Taylor JM**. 2017. LOCALIZER: subcellular localization prediction of both plant
1079 and effector proteins in the plant cell. *Scientific Reports*. 2017 Mar 16;7:44598. doi:
1080 10.1038/srep44598. PMID: 28300209; PMCID: PMC5353544.
1081 **Stergiopoulos I, Kourmpetis YA, Slot JC, Bakker FT, de Wit PJGM, Rokas A**. 2012. In
1082 silico characterization and molecular evolutionary analysis of a novel superfamily of
1083 fungal effector proteins. *Molecular Biology and Evolution*. 2012 Nov;29(11):3371-84.
1084 doi: 10.1093/molbev/mss143. Epub 2012 May 23. PMID: 22628532.
1085 **Sushida H, Sumita T, Higashi Y, Iida Y.** 2019. Draft Genome Sequence of *Dicyma*
1086 *pulvinata* Strain 414-3, a Mycoparasite of *Cladosporium fulvum*, Causal Agent of
1087 Tomato Leaf Mold. *Microbiology Resource Announcements*. 2019 Aug 29;8(35):e00655-
1088 19. doi: 10.1128/MRA.00655-19. PMID: 31467096; PMCID: PMC6715866.
1089 **Tanaka S, Wada K, Katayama M, Marumo S**. 1984. Isolation of Sporogen-AO1, a
1090 sporogenic substance, from *Aspergillus oryzae*. A*gricultural and biological chemistry*.
1091 1984;48(12):3189–3191. doi:10.1271/bbb1961.48.3189.
1092 **Tanaka S, Wada K, Marumo S, Hattori H.** 1984. Structure of sporogen-ao 1, a sporogenic
1093 substance of *Aspergillus oryzae*. *Tetrahedron Letters*. 1984;25(51):5907–5910.
1094 doi:10.1016/S0040-4039(01)81717-2.

1095 **Tang D, Chen M, Huang X, Zhang G, Zeng L, Zhang G, Wu S, Wang Y.** 2023. SRplot:
1096 A free online platform for data visualization and graphing. *PLoS One*. 2023 Nov
1097 9;18(11):e0294236. doi: 10.1371/journal.pone.0294236. PMID: 37943830; PMCID:
1098 PMC10635526.
1099 **Teufel F, Almagro Armenteros JJ, Johansen AR, Gíslason MH, Pihl SI, Tsirigos KD,**
1100 **Winther O, Brunak S, von Heijne G, Nielsen H.** 2022. SignalP 6.0 predicts all five
1101 types of signal peptides using protein language models. *Nature Biotechnology*. 2022
1102 Jul;40(7):1023-1025. doi: 10.1038/s41587-021-01156-3. Epub 2022 Jan 3. PMID:
1103 34980915; PMCID: PMC9287161.
1104 **Thomma BP, van Esse HP, Crous PW, de Wit PJGM.** 2005. *Cladosporium fulvum* (syn.
1105 *Passalora fulva*), a highly specialized plant pathogen as a model for functional studies on
1106 plant pathogenic Mycosphaerellaceae. *Molecular Plant Pathology*. 2005 Jul 1;6(4):379-
1107 93. doi: 10.1111/j.1364-3703.2005.00292.x. PMID: 20565665.
1108 **Tirilly Y, Kloosterman J, Sipma G, Kettenes-Van Den Bosch JJ.** 1983. A fungitoxic
1109 sesquiterpene from *Hansfordia pulvinata*. *Phytochemistry*. 1983;22(9):2082–2083.
1110 doi:10.1016/0031-9422(83)80051-X.
1111 **Tünnermann L, Colou J, Näsholm T, Gratz R.** 2022. To have or not to have: expression of
1112 amino acid transporters during pathogen infection. *Plant Molecular Biology*. 2022
1113 Jul;109(4-5):413-425. doi: 10.1007/s11103-022-01244-1. Epub 2022 Feb 1. PMID:
1114 35103913; PMCID: PMC9213295.
1115 **Watanabe H, Horinouchi H, Muramoto Y, Ishii H.** 2017. Occurrence of azoxystrobin-
1116 resistant isolates in *Passalora fulva*, the pathogen of tomato leaf mold disease. *Plant*
1117 *Pathology*. 2017;66(9):1472–1479. doi:10.1111/ppa.12701.
1118 **Wulff BB, Chakrabarti A, Jones DA.** 2009. Recognitional specificity and evolution in the
1119 tomato-*Cladosporium fulvum* pathosystem. *Molecular Plant-Microbe Interactions*. 2009
1120 Oct;22(10):1191-202. doi: 10.1094/MPMI-22-10-1191. PMID: 19737093.
1121 **Yan L, Chen J, Zhang C, Ma Z.** 2008. Molecular characterization of benzimidazole-
1122 resistant isolates of *Cladosporium fulvum*. *Fems Microbiology Letters*. 2008
1123 Jan;278(2):242-8. doi: 10.1111/j.1574-6968.2007.00999.x. PMID: 18096020.
1124 **Yang K, Chen C, Wang Y, Li J, Dong X, Cheng Y, Zhang H, Zhai Y, Ai G, Song Q**, et
1125 al. 2022. Nep1-Like Proteins From the Biocontrol Agent *Pythium oligandrum* Enhance
1126 Plant Disease Resistance Independent of Cell Death and Reactive Oxygen Species.
1127 *Frontiers in Plant Science*. 2022 Mar 4;13:830636. doi: 10.3389/fpls.2022.830636.
1128 PMID: 35310640; PMCID: PMC8931738.

1129 **Zaccaron AZ, Stergiopoulos I.** 2024. Analysis of five near-complete genome assemblies of
1130 the tomato pathogen *Cladosporium fulvum* uncovers additional accessory chromosomes
1131 and structural variations induced by transposable elements effecting the loss of
1132 avirulence genes. *BMC Biology*. 2024 Jan 29;22(1):25. doi: 10.1186/s12915-024-01818-
1133 z. PMID: 38281938; PMCID: PMC10823647.
1134 **Zaccaron AZ, Chen LH, Samaras A, Stergiopoulos I.** 2022. A chromosome-scale genome
1135 assembly of the tomato pathogen *Cladosporium fulvum* reveals a compartmentalized
1136 genome architecture and the presence of a dispensable chromosome. *Microbial*
1137 *Genomics*. 2022 Apr;8(4):000819. doi: 10.1099/mgen.0.000819. PMID: 35471194;
1138 PMCID: PMC9453070.
1139 **Zhang H, Yohe T, Huang L, Entwistle S, Wu P, Yang Z, Busk PK, Xu Y, Yin Y.** 2018.
1140 dbCAN2: a meta server for automated carbohydrate-active enzyme annotation. *Nucleic*
1141 *Acids Research*. 2018 Jul 2;46(W1):W95-W101. doi: 10.1093/nar/gky418. PMID:
1142 29771380; PMCID: PMC6031026.
1143 **Zhang Y, Skolnick J.** 2005. TM-align: a protein structure alignment algorithm based on the
1144 TM-score. *Nucleic Acids Research*. 2005 Apr 22;33(7):2302-9. doi: 10.1093/nar/gki524.
1145 PMID: 15849316; PMCID: PMC1084323.
1146 **Zhou BJ, Jia PS, Gao F, Guo HS.** 2012. Molecular characterization and functional analysis
1147 of a necrosis- and ethylene-inducing, protein-encoding gene family from *Verticillium*
1148 *dahliae*. *Molecular Plant-Microbe Interactions*. 2012 Jul;25(7):964-75. doi:
1149 10.1094/MPMI-12-11-0319. PMID: 22414440.
1150

1151 **FIGURE LEGENDS**

1152 **Fig. 1. *Cladosporium fulvum* parasitized by mycoparasitic fungus *Hansfordia pulvinata*.**
1153 (a) Representative images of a healthy tomato leaf, lesions caused by *C. fulvum* (*in planta*
1154 *Cf*), and lesions covered by white mycelium of *H. pulvinata* (*in planta Cf/Hp*). Tomato plants
1155 were inoculated with *C. fulvum*, and lesions developed after 2 weeks. *H. pulvinata* was then
1156 inoculated onto the diseased leaves, and white mycelia appeared on the lesions a week after
1157 the second inoculation. *In vitro* cultures of *H. pulvinata* (*in vitro Hp*) and *C. fulvum* (*in vitro*
1158 *Cf*) on nylon membranes on water agar after transfer from PDA. *H. pulvinata* parasitized *C.*
1159 *fulvum* colonies on water agar (*in vitro Cf/Hp*). (b) Scanning electron micrographs of hyphae
1160 of *C. fulvum* and *H. pulvinata* in *in vitro Cf* and *Cf/Hp* conditions. *H. pulvinata* hyphae have
1161 penetrated *C. fulvum* hyphae in the *in vitro Cf/Hp* condition. Bar indicates 10 μm.
1162

1163 **Fig. 2. Differentially expressed genes (DEGs) and enriched KEGG pathways in**
1164 **mycoparasite *Hansfordia pulvinata*.** (a) UpSet plot of DEGs in the *in vitro* and *in planta*
1165 mycoparasitic conditions (*in vitro Cf/Hp* and *in planta Cf/Hp*; Fig. 1a). Connected dots
1166 indicate shared DEGs; Black single dots represent condition-specific DEGs. Vertical bars
1167 show the number of up- and downregulated genes; colored horizontal bars indicate the total
1168 number of DEGs detected in each interaction. (b) Bubble plot of KEGG pathway enrichment
1169 analysis based on the 891 and 557 shared DEGs shown in (a). Keys: color of symbols
1170 indicates significance level of enrichment (–log adjusted *P*); size of symbol indicates the
1171 number of enriched DEGs in each pathway; the symbol indicates the functional class of the
1172 enriched DEGs.
1173
1174 **Fig. 3. A Nep1-like protein (NLP) secreted from the mycoparasite *Hansfordia pulvinata***
1175 **induces a plant-mediated toxicity against spores of *Cladosporium fulvum*.** (a) Workflow
1176 for identifying small secreted proteins synthesized in *H. pulvinata* during mycoparasitism. (b)
1177 MA plot for expression levels of 165 selected genes. Cutoff thresholds are $\log_2$ Fold-change
1178 (±1.0) for *in vitro Cf/Hp* interaction and log Mean (0.3). (c) Phylogenetic tree constructed
1179 based on NLP amino acid sequences using the maximum likelihood method with 1,000
1180 bootstrap replicates. Type I and Type II have two and four cysteine residues, respectively.
1181 Proteins analyzed in this study are in bold. (d) Multiple sequence alignment of NLP using
1182 MAFFT. Conserved residues are highlighted in orange. (e) Transient expression assays of
1183 NLPs in *Nicotiana benthamiana* via agroinfiltration. Chlorosis and necrosis were assessed 14
1184 days after infiltration by trypan blue staining. Similar results were obtained in three
1185 independent experiments; representative results are in Supplementary Fig. S5c. (f) Percentage
1186 germination of conidia of *C. fulvum* after 24-h treatment with apoplastic fluid from *N.*
1187 *benthamiana* leaves that had been infiltrated with different NLPs or buffer. Asterisks indicate
1188 significant differences between treatments determined using Dunnett's or the Mann–Whitney
1189 *U* test.
1190
1191 **Fig. 4. Differentially expressed genes (DEGs) and enriched KEGG pathways in the**
1192 **pathogen *Cladosporium fulvum*.** (a) UpSet plot showing DEGs identified in the *in planta Cf,*
1193 *in vitro Cf/Hp,* and *in planta Cf/HP* conditions (see Fig. 1A). Connected dots indicate shared
1194 DEGs; Black single dots represent condition-specific DEGs. Vertical bars show the numbers
1195 of up- and downregulated genes; colored horizontal bars indicate the total number of DEGs
1196 detected in each condition. (b) Bubble plot of KEGG pathway enrichment analysis based on

1197 the 363 and 158 shared DEGs shown in (a). Keys: color of symbols indicates significant level
1198 of enrichment (–log adjusted *P*); size of symbol indicates the number of enriched DEGs in
1199 each pathway; the symbol indicates the functional class of the enriched DEGs.
1200
1201 **Fig. 5. Effector genes in the pathogen *Cladosporium fulvum* were highly expressed**
1202 **during mycoparasitism by *Hansfordia pulvinata.*** (a) Functional classification of DEGs
1203 identified for the *in planta Cf*, *in vitro Cf/Hp* and *in planta Cf/Hp* interactions. Red:
1204 upregulated, stable: grey, blue: downregulated. The number of genes assigned to each
1205 category is in parentheses. (b) Heatmap showing expression profiles of effector genes. The
1206 red-to-blue gradient represents up- and downregulated expression, respectively. Genes with
1207 an adjusted *P*-value ≥0.05 are indicated in gray as not detected (ND). Red arrowhead
1208 indicates *Ecp2*. (c) Antimicrobial activity prediction for 56 effector genes upregulated during
1209 the *in vitro Cf/Hp* interaction (determined using the AMAPEC program). Symbols denote
1210 protein location predicted by EffectorP-fungi 3.0.
1211
1212 **Fig. 6. Sequence dissimilarity and structural similarity between *Cladosporium fulvum***
1213 **effector Ecp2 and killer toxin KP4 proteins.** (a) Predicted 3D structure of Ecp2 generated
1214 using AlphaFold2. The color spectrum from blue to red indicates the N- to C-terminal
1215 positions of residues. (b) Structural comparison of Ecp2 with ZtKP4 and UmVKP4 proteins.
1216 The superposition of the aligned proteins was evaluated using TM-align, and the TM-score
1217 and RMSD values are shown. (c) Heatmap showing sequence similarity among Ecp2, ZtKP4,
1218 and UmVKP4 proteins as identified by BLASTp analysis. (d) Conserved motifs of
1219 the proteins identified by MEME motif analysis. (e) Representative tomato leaf from 4-week-
1220 old tomato plant carrying the *Cf-ECP2* resistance gene at 6 days after infiltration with
1221 purified Ecp2 protein produced by *Escherichia coli*. White dotted outline: area infiltrated
1222 with infiltrated with 1 μM Ecp2; black dotted outline: infiltrated with control protein purified
1223 from *E. coli* harboring an empty vector (EV). Numbers in parentheses indicate the number of
1224 leaves with a hypersensitive response (HR) relative to the number of total leaves. (f) *In vitro*
1225 antifungal activity of Ecp2 against *C. fulvum*, *H. pulvinata*, *Alternaria* sp., *Colletotrichum*
1226 *orbiculare*, and *Saccharomyces cerevisiae*. Spores were cultured on 5% potato dextrose agar
1227 with or without Ecp2. Relative hyphal length was determined 4 days after treatment. Bars =
1228 250 μm. Significant differences between EV and Ecp2 treatments were assessed using
1229 Student's t-test, and *P*-values are indicated.
1230

1231 **Fig. 7. Differentially expressed genes (DEGs) and enriched KEGG pathways in tomato**
1232 **plants.** (a) UpSet plot of DEGs in the *in planta Cf* and *in planta Cf/Hp* conditions (see Fig.
1233 1a). Healthy leaves were used as a control. Connected dots indicate shared DEGs; Black
1234 single dots represent condition-specific DEGs. Vertical bars show the number of up- and
1235 downregulated genes; colored horizontal bars indicate the total number of DEGs detected in
1236 each interaction. (b) Bubble plot of KEGG pathway enrichment analysis based on the 1,619
1237 and 2,153 DEGs shown in (a). Keys: color of symbols indicates significance level of
1238 enrichment (–log adjusted *P*); size of symbol indicates the number of enriched DEGs in each
1239 pathway; the symbol indicates the functional class of the enriched DEGs. Stars indicate
1240 pathways highlighted in (c). (c) KEGG pathways involved in amino acid biosynthesis in
1241 tomato.
1242
1243 **Fig. 8. Overview of the tripartite interaction among tomato plants, pathogen**
1244 ***Cladosporium fulvum*, and mycoparasite *Hansfordia pulvinata*.** *C. fulvum* secretes effector
1245 proteins that function as virulence factors in susceptible tomato cultivars and antifungal
1246 proteins active against other fungi, but act as avirulence factors upon recognition by *Cf*-
1247 resistant cultivars. *H. pulvinata* parasitizes *C. fulvum* and induces the production of apoplastic
1248 antifungal substances in tomato plants via the Nep1-like protein HpNlp1. *H. pulvinata* also
1249 activates the biosynthesis of the antifungal sesquiterpene 13-deoxyphomenone during
1250 mycoparasitism. Other plant defense responses support this biocontrol effect. Pathways
1251 related to amino acid biosynthesis in the three organisms suggest that nutrients from the plant
1252 are supplied to *H. pulvinata*.
1253
1254 **SUPPORTING INFORMATION**
1255 **Fig. S1** Experimental treatments and principal component analysis (PCA) of transcripts from
1256 the mycoparasite *Hansfordia pulvinata* (Hp), the pathogen *Cladosporium fulvum* (Cf), and
1257 tomato plant, *Solanum lycopersicum*.
1258 **Fig. S2** Secondary metabolite biosynthesis gene clusters in the mycoparasite *Hansfordia*
1259 *pulvinata*.
1260 **Fig. S3** Phylogenetic analysis and functional characterization of proteins in fungal species.
1261 **Fig. S4** Structure of HpNlp1.
1262 **Fig. S5** Responses in plant leaves triggered by HpNlp1 protein.
1263 **Fig. S6** Heat map and hierarchical clustering of effector genes expressed in *Cladosporium*
1264 *fulvum*.

1265 **Fig. S7** Structural comparative analysis of Ecp2 with ZtKP4 and UmVKP4.

1266 **Fig. S8** Differentially expressed genes (DEGs) in KEGG pathways detected in tomato plants.

1267 **Table S1** Primer sequences used in this study.

1268 **Table S2** Summary statistics of RNA-seq data and mapping results.

1269 **Table S3** Functional annotation of all genes in *Hansfordia pulvinata* genome.

1270 **Table S4** Predicted gene clusters involved in secondary metabolite biosynthesis in

1271 *Hansfordia pulvinata*.

1272 **Table S5** Small secreted protein-coding genes (≤300 aa) in *Hansfordia pulvinata*.

1273 **Table S6** Key genes encoding secondary metabolism enzymes in *Cladosporium fulvum*.

1274 **Table S7** Effector genes identified in *Cladosporium fulvum*.

1275 **Table S8** Structural homologs of Ecp2 protein identified from PDB25 using the Dali server.

1276 **Table S9** Species possessing homologs of Ecp2 and KP4 proteins.

1277 **Table S10** Log_2 fold-change for defensin-like genes in tomato plants.